2005

Investigations On Rf Sputter Deposited Sicn Thin Films For Mems Applications

Ravi Todi
University of Central Florida

INVESTIGATIONS ON RF SPUTTER DEPOSITED SiCN THIN FILMS FOR MEMS APPLICATIONS

by

RAVI M. TODI
B.E.E.E. Mumbai University, 2002
M.S.E.E., University of Central Florida, 2004

A thesis submitted in partial fulfillment of the requirements
for the degree of Master of Science
in the Department of Mechanical Materials and Aerospace Engineering
in the College of Engineering and Computer Science
at the University of Central Florida
Orlando, Florida

Fall Term
2005

ABSTRACT

With the rapid increase in miniaturization of mechanical components, the need for a hard, protective coatings is of great importance. In this study we investigate some of the mechanical, chemical and physical properties of the SiCN thin films. Thin films of amorphous silicon carbide nitride (a-SiC_xN_y) were deposited in a RF magnetron sputtering system using a powder pressed SiC target. Films with various compositions were deposited on to silicon substrate by changing the N_2/Ar gas ratios during sputtering. Nano-indentation studies were performed to investigate the mechanical properties such as hardness and reduced modulus of the SiCN films. Surface morphology of the films was characterized by using atomic force microscopy (AFM). X-ray photoelectron spectroscopy (XPS) data indicated that the chemical status is highly sensitive to the nitrogen ratios during sputtering. Further, the films were annealed in dry oxygen ambient in the temperature range of 400 – 900°C and characterized using XPS to investigate the chemical composition and oxidation kinetics at each annealing temperature. The surface roughness of these films was studied as a function of annealing temperature and film composition with the help of a ”Veeco” optical profilometer.

Nano-indentation studies indicated that the hardness and the reduced modulus of the film are sensitive to the N_2/Ar ratio of gas flow during sputtering. AFM studies revealed that the films become smoother as the N_2/Ar ratio is increased. XPS data indicated the existence of C-N phases in the as-deposited films. The study of oxidation kinetics of RF sputter deposited SiCN thin films, using XPS, suggest that N_2 co-sputtering helps to suppress the formation of a surface oxide, by allowing un-bonded Si to bond with N and C inside the vacuum chamber as opposed to bonding with O in atmosphere.

dedicated to my grandparents

Shri Ramlal Todi

Late Smt. Mohini Devi Todi

who have always been inspirational sources in helping me realize my goals

ACKNOWLEDGMENTS

First and foremost, I would like to acknowledge and thank my advisors Dr. Kevin R. Coffey and Dr. Kalpathy B. Sundaram for their guidance and support which was crucial for the completion of this work. Thanks to Dr. Quanfang Chen for serving on my thesis committee and for his valuable advice and comments that helped me improve the quality of my thesis.

I am grateful to Edward Dein for giving me my first lessons in the cleanroom and for helpful suggestions at all times. I also wish to acknowledge Advanced Microfabrication Facility and the Materials Characterization Facility at the Advanced Materials Processing and Analysis Center for laboratory support.

I would like to thank my colleague Mr. Arun Vijayakumar, who helped me tremendously throughout all the experiments and for guiding me through the tedious task of putting this thesis document together. Thanks are due to my friend and colleague Andrew Warren for help with XPS analysis. In addition, I would like to acknowledge Hysitron Incorporated for nano-indentation analysis and Dr. Du, for help with AFM measurements. At this time I would also like to acknowledge all my peers for their valuable suggestions at all times. Finally, with deep gratitude, I would like to thank my parents, family and friends for their love and moral support.

TABLE OF CONTENTS

LIST OF FIGURES

LIST OF TABLES

LIST OF ACRONYMS/ABBREVIATIONS

ACRONYM	Definition of Acronym
MEMS	Micro-Electro-Mechanical System
SiCN	Silicon-Carbon-Nitride
UHV	Ultra High Vacuum
AFM	Atomic Force Microscopy
XPS	X-ray Photoelectron Spectroscopy
UHP	Ultra High Pure
RF	Radio Frequency
AES	Auger Electron Spectroscopy
SIMS	Secondary Ion Mass Spectroscopy
BE	Binding Energy
DI	De-Ionized
RMS	Root Mean Square

CHAPTER ONE: INTRODUCTION

There is a constant demand for increased levels of performance for any kind of system. This is more pronounced in the high-tech age that we are in now. With more and more applications driving their respective technology to the maximum performance level, it is obvious that the current technology will reach a saturation point. Hence it becomes essential that we come up with new materials and designs that can meet and surpass current performance levels. The demand for tough materials which have high hardness and are resistant to a variety of harsh environments has been increasing for the past few decades. Especially in situations where the material is required in the form of thin films, such as protective hard coatings, micro or nano-scale non-intrusive sensors and harsh environment devices, the development of new materials that can outperform currently available materials is essential to keep up with increasing performance level demands. This thesis work examines some of the mechanical, chemical and physical properties of SiCN thin films, that can be used a protective hard coating for MEMS applications.

The aim of the present work is to investigate some of the mechanical, chemical and physical properties of SiCN films. Thin films of amorphous silicon carbide nitride (a-SiC_xN_y) were deposited in a RF magnetron sputtering system using a powder pressed SiC target. Films with various compositions were deposited on to silicon substrates by changing the N_2/Ar gas ratio during sputtering. The films were then characterized by various techniques, including nano-indentation, atomic force microscopy (AFM), X-ray photoelectron spectroscopy (XPS), and optical profilometry. A brief outline of the rest of the chapters is as follows:

Chapter 2 consists of a literature survey of the work done by various investigators on the techniques of making SiC_xN_y films, and properties of SiC_xN_y films.

Chapter 3 describes the actual experimental process for obtaining and characterizing amorphous SiC_xN_y thin films in the present work. This chapter provides details on the sputter deposition technique and the various characterization techniques such as nano-indentation, AFM and XPS used in this work. It also briefly describes the Veeco optical profilometer, used in the present work for surface roughness measurements.

Chapter 4 is the core of this thesis and includes results and discussions. This chapter provides an insight in to the properties of the SiCN thin films investigated in this work. Here we provide detailed discussion of the results obtained from various characterization techniques. This chapter contains two sections, with first describing the characteristics of the as deposited films, and the second section describing the properties of the SiCN films after dry oxygen annealing in the temperature range of 400 – 900 °C.

Chapter 5 summarizes the present work.

CHAPTER TWO: LITERATURE REVIEW

Initial work on tough materials was inspired by studies on the hardness of the materials. The hardness of a material is related to its bulk modulus, *B* and is influenced microscopically by point defects, dislocations, the structure of grain boundaries in nano-or polycrystalline materials, the crystallite size and the porosity [1]. Liu and Cohen [2, 3] made a very significant theoretical prediction, that β-C_3N_4 which is isomorphic with β-Si_3N_4 can possess a bulk modulus which can surpass that of diamond. They developed an empirical equation that describes the bulk modulus of materials using scaling relationships.

$$B = \frac{\langle N_c \rangle}{4} \frac{1971 - 220.\lambda}{d^{3.5}}$$

Where *B* is the bulk modulus in GPa, N_c is the average coordination number, *d* is the bond length in Å and λ is a parameter describing the ionicity of the chemical bonding. Thus, solids with small covalent bonds exhibit the highest bulk moduli (*d* small, λ = 0). Further it can be concluded that the lower the bond length of the material, the higher the bulk modulus and thus the hardness. Diamond has the lowest known bond length of 1.54 Å and consequently the highest bulk modulus of about 435GPa [4]. Only the hypothetical material β-C_3N_4 is expected to be harder on the basis of the above equation. This has inspired research in the development of C_3N_4 over the past two decades. In addition to hardness, the C-N material is expected to possess wide bandgap, high thermal conductivity, high strength, high decomposition temperature, and excellent resistance to corrosion and wear. More recently binary, ternary and quaternary carbonitride materials such as CN_x, BCN, SiCN, SiBCN and AlBCN have been investigated and found to be of significant interest to industry owing to their light weight and multi-functional

properties [5]. Gomez et al. [6] suggested that if β-Si_3N_4 and β-C_3N_4 have the same structure, it might be expected that both should be miscible giving rise to SiCN alloys. Miyagawa et al. [7] have demonstrated that nitrogen-ion implantation in silicon carbide produces a surface layer with an intermediate state SiC_xN_y or into Si_3N_4 under appropriate conditions. Further studies on such films have revealed them to be thermally stable to certain temperatures, but at higher temperatures it was observed that nitrogen present in interstitial states is lost [8]. Bendeddouche et al. [9] stated that the properties of this new material could be an interesting combination of silicon carbide, a semiconductor, and silicon nitride, a dielectric. In other words, it might be a hard material with a wide band gap having interesting optical and electronic properties.

Considerable efforts have been made to synthesize SiCN films by different techniques including electron cyclotron resonance (ECR) and plasma enhanced chemical vapor deposition (PECVD) [10, 11]. Soto et al. [12] have deposited amorphous SiC_xN_y films by pulse laser deposition on single crystal silicon substrate by KrF excimer laser ablation of a SiC sintered target in a vacuum system at room temperature using non-reactive Ar and reactive N_2 background gases at different pressures. Chen et al. [13] reported on the growth and mechanical properties of large (several tens of microns), well-faceted ternary SiCN crystals grown by microwave plasma-enhanced chemical vapor deposition, and amorphous SiCN films grown by ECR-CVD. They employed nano-indentation studies to investigate the mechanical properties of the SiCN materials. More recently Cheng et al studied the morphology and bonding structure of SiCN films deposited using microwave plasma CVD by varying film composition through the N_2 flow rate and temperature. They report that higher substrate temperatures facilitate crystallization and larger crystalline size [14]. Other techniques used to synthesize CN alloys are reactive sputtering [15, 16] and ion assisted dynamic mixing [17]. Carbon–silicon–nitride thin films were

grown on (100) oriented silicon using pulsed laser deposition (PLD) assisted by a RF nitrogen plasma source by Tharigen et al. [18]. They found that due to incorporation of 10% Si_3N_4 to the PLD graphite target the CSi_xN_y films show slightly increased hardness value of 23 GPa (reference value for silicon substrate 14 GPa), but strongly decreased elastic modulus from 464 to 229 GPa. Lowther et al. used *ab initio* and self-consistent-charge density functional based tight-binding electronic structure calculations and assessed the possibility that synthesized layered structure of Si_2CN_4 can lead to super-hard structures in the spinel or the β phase [19].

Lehmann et. al. deposited amorphous SiC_xN_y films with various compositions by ion beam sputtering and observed the decrease in Young's modulus with increase in carbon content [20]. The hardness and effective modulus of hydrogen-containing and hydrogen-free amorphous CSi_xN_y films, deposited by electron cyclotron resonance plasma chemical vapor deposition (ECR-CVD) and hydrogen free ion-beam sputtering deposition (IBSD), respectively, were studied through nano-indentation by Lo et al. [21]. Yamamoto et al. formed amorphous SiCN films on Si(1 0 0) substrate by nitrogen ion-assisted pulsed-laser ablation of an SiC target and the dependence of the formed chemical bonds in the films on nitrogen ion energy and substrate temperature were investigated by XPS [22]. In a more recent publication Bruns et al. [23] report the deposition of thin SiCN films using RF sputtering combined with ion implantation. They claim that it is an effective technique to produce nitrogen rich high purity SiCN films. However it was found that the region of attainable stoichiometries is narrowed by formation of Si-C-N phases and N_2, respectively.

According to Lutz et al [24], for the reproducible production of SiCN thin films with tailored stoichiometries and high-purity, RF magnetron spurring and ion implantation are very promising techniques. Also magnetron sputtering is the most versatile technique when it comes

to deposition of a wide range of materials with practically no restrictions on the type of substrate to be used. Wei at al. [25], used DC magnetron sputtering with RF biasing to deposit SiCN films from silicon and graphite planar targets under a N_2- Ar ambient. It was found that the N_2 fraction in the gas mixture has a major influence on the deposition rate and composition of the films: a high N_2 fraction results in increased deposition rate and N/(C+Si) and C/(N+Si) ratios. They found that the SiCN films deposited were amorphous with chemical analysis showing the existence of Si – N, C – N single, C = N double and C ≡ N triple bonds. Almost no Si – C bonding was found in the films. Analysis of bonding structures in chemical vapor deposited SiCN films, performed by Bendeddouche et al. [9] indicate the presence of Si – C bonds in addition to Si – N, C – C and C – N bonds. This shows that there could be a difference in structure between films due to different deposition methods. RF magnetron sputter deposition technique was applied by Sundaram et al. [26] where a powder pressed SiC target was used under N_2+Ar ambience, instead of the two target method used by Wei et al. They studied the optical absorption characteristics of the SiCN films using FTIR spectroscopy. It was found that the band gap of the films increased with increase in N_2/Ar ratios and the percentage of optical transmission also increased with the N_2/Ar ratio. Amorphous silicon carbonitride (a-SiCN) films were synthesized by Ming He at al. [27] by ion enhanced RF magnetron sputtering from a Si_4C target using a mixture of Ar and N_2 gases. The oxidation resistance of the films was investigated in an oxygen atmosphere over the temperature range of 0–1000 ◦C. X-ray photoelectron spectroscopy showed that the SiCN films exhibited a well-defined Si–C–N bonding structure. The composition, density, hardness, and stress were uniquely characterized with respect to the average energy per deposited atom. It was demonstrated that under optimum deposition

conditions a-SiCN films can be prepared to exhibit high density (>2.6 g cm−3), high hardness (>25 GPa), and enhanced oxidization resistance at temperatures up to 800 ◦C.

Wu et al. [28] obtained SiCN films by RF sputtering with a highly pure polycrystalline silicon target and a gaseous ambient comprising of Ar, N_2, H_2 and CH_4. Their studies on the electrical conductivity of the films indicate a decrease in conductivity with increase in N_2 flow ratio. They also found their films to be thermally stable at high temperatures and attribute this to the coexistence of carbon and nitrogen in the films. Xie et al. [28] studied varying substrate temperature characteristics of SiCN films during deposition by RF sputtering from a SiC target in N_2+ Ar gas ambient. It was observed that the growth rate of SiCN films increases with growth temperature. Analysis of the films suggests a variation in chemical bonding states of the SiCN films with deposition temperature. The carbon content in the SiCN film was observed to increase while that of nitride decreased with the increasing substrate temperature. Hence, they conclude that high substrate temperature is not favorable for nitrogen incorporation into SiCN films.

SiCN has a wide range of applications due to its properties. One of the earliest applications, proposed by Misaki at al. [30] used SiCN as protective films for magneto-optical media. SiCN is finding increasing application in the semiconductor device industry as a candidate for high voltage SiCN/Si heterojunction diodes for high temperature applications [31]. Another interesting and promising area is in the fabrication of microelectromechanical (MEMS) systems for harsh environments where SiCN could prove as a good candidate. A simple SiCN MEMS thermal actuator was demonstrated by Liew et al [32]. However, their structure was built on bulk SiCN ceramic material obtained from a polymer precursor. Hence, the development of MEMS structures based on sputtered high quality SiCN thin films is still open to research.. Of special interest are SiCN films deposited by RF sputtering due to the many advantages that

sputtering provides over other techniques, such as the freedom to choose substrate material, a uniform deposition over relatively larger area and the possibility to vary the composition of N_2 gas to prepare SiCN film of various compositions. Thus, the focus of this thesis is to make a detailed study of the characteristics of SiCN thin films deposited by reactive RF sputtering and provide a broader understanding about the properties of these films.

CHAPTER THREE: METHODOLOGY

3.1 Sample Prep: Thin Film Deposition

Thin films of SiCN were deposited by reactive RF magnetron sputtering in an ultra high vacuum (UHV) deposition system. A 2 inch, powder pressed, SiC target with a purity of 99.5% was used. The system base pressure was approximately 1 X 10^{-8} Torr and the purity of the process gas was maintained by a hot reactive metal getter. Process gas contamination in the deposition chamber at the typical deposition pressure of 4 mTorr was confirmed to be less than 10 ppm (the instrumental sensitivity limit) by closed ion source quadrapole mass spectrometry. The N_2 to Ar ratio was varied from 0 to 1, in steps of 0.25 by changing the individual gas flow rate, while the total gas flow was kept constant at 20 sccm and a constant deposition pressure of 4 mTorr. These samples were then characterized by different techniques including nano-indentation, AFM and XPS, to be described in later part of this chapter.

Samples were also annealed in an ultra high purity (UHP) O_2 ambient in the temperature range of 400°C to 900°C in a box furnace, to study the oxidation kinetics of the SiCN thin films. A total of 30 samples were made with five compositions based on different N_2/Ar ratios and six annealing temperatures in the range of 400°C to 900°C. The sample matrix is given below in Table 3.1. The oxygen annealed samples were then characterized by XPS to study the chemical status, and the surface roughness was analyzed by using a "Veeco" optical profilometer, to be described in details later. Before moving in the details of characterizations, I first present a brief over view of the sputtering processed used in the present research work.

Table 3.1: Sample matrix describing different N_2/Ar ratios and annealing temperatures.

Temp. / N_2/Ar	400°C	500°C	600°C	700°C	800°C	900°C
0.00 (SiC)	1.1	1.2	1.3	1.4	1.5	1.6
0.25 (SiCN)	2.1	2.2	2.3	2.4	2.5	2.6
0.50 (SiCN)	3.1	3.2	3.3	3.4	3.5	3.6
0.75 (SiCN)	4.1	4.2	4.3	4.4	4.5	4.6
1.00 (SiCN)	5.1	5.2	5.2	5.4	5.5	5.6

3.1.1 Sputtering Overview

Sputtering is the removal of material from a solid target by energetic ion bombardment. When the sputtered material is used to coat a substrate this is called sputter deposition.

Sputter deposition sources (also called sputter "guns") create a low pressure plasma by the excitation of an inert gas (typically argon) contained at 1 to 30 millitorr in a vacuum chamber. This process extracts energetic ions which accelerate toward the cathode target, striking it with kinetic energy up to several hundred eV. Energy transfer then ejects material from the target with approximately 90% leaving as neutral atoms and 10% as ions. Gas phase collisions between target atoms and argon atoms scatter the ejected material into a distributed cloud. As the cloud migrates towards the substrate, the random approach angles result in deposition of a uniform film, even on surfaces that have micron-sized vertical structures. Described below are some of the main variations of a typical sputter deposition technique.

3.1.1.1 DC Diode Sputtering

This older technique is not used much because high operating pressures are required. The higher pressures not only present problems for the vacuum pumps but also results in a severe rate and efficiency loss due to gas phase scattering of the sputtered material.

3.1.1.2 RF Diode Sputtering

RF power is coupled to the powered electrode through a blocking capacitor. The discharge plasma "acts like" a rectifier and the capacitor is charged to a negative voltage known as the DC Bias Potential. This DC bias potential is generally a reasonable measure of the kinetic energy of the bombarding ions that actually perform the sputtering. Substrate bombardment by energetic electrons is often a practical limitation, but the technique still has many practical applications.

3.1.1.3 Ion Beam Sputtering

This technique makes use of broad beam ion sources. One advantage of the technique is that the source of ions, the sputter target and the substrate are decoupled. This allows a high degree of independent control. The downside of the technique is that the broad beam ion sources themselves are somewhat fragile.

3.1.1.4 DC and RF Magnetron Sputtering

This is a crossed field plasma device that not only reduces impedance and permits operation at relatively low pressure but also substantially reduces substrate bombardment. A wide variety of these sputter sources exist. The high deposition rates result from the high power that can be applied at nearly optimal target potentials. RF Magnetron sputter sources operate in much the same manner as DC Magnetron sputter sources. There are, however, some important complicating factors and the operating point for the RF magnetron source is generally located at a higher potential than that of the DC magnetron source. RF magnetron sputtering techniques have been used for this thesis work. A brief description and physics of magnetron source is given in the next section.

3.1.2 Magnetron Source

The most common used sputter source in current use is a magnetron sputter source. Magnetron sources vary widely in their construction geometry but the most common arrangement is the planar magnetron source. A planar magnetron source is a planar diode source with an array of magnets added behind the cathode (target) surface. These magnets generate a magnetic field of around 50-500 gauss parallel to the target surface. Planar magnetrons have been designed for a variety of shapes but the circular shape is the most commonly used as it matches the circular geometry of the wafer.

The combination of an electric field and a magnetic field results in trapping of electrons and causes them to drift in a closed loop in front of the target surface. The drift of the electrons is

in –E x B direction due to "Hall Effect" but superimposed on this drift is cycloidal motion as shown in Fig. 3.1. The gyroscopic radius of the electron orbits is given by

$$\rho = m\upsilon_{\perp} / qB$$

where $\upsilon_{\perp}$ is the component of the electron velocity that is perpendicular to the flux lines, m and q are the mass and charge on the electron respectively and B is the magnetic field. This radius is typically of the order of a few millimeters or less for most sputtering systems. An electron encircles the lines of flux until it is scattered by another particle. Practically, a magnetron exists when the –E x B path is closed and the electrons remain trapped for several trips around the loop.

This confinement of electrons results in enhanced ion bombardment and sputtering rates for both DC and RF discharges. In general, a magnetron discharge is much more efficient, with either DC or RF excitation, than one that does not utilize magnetic trapping.

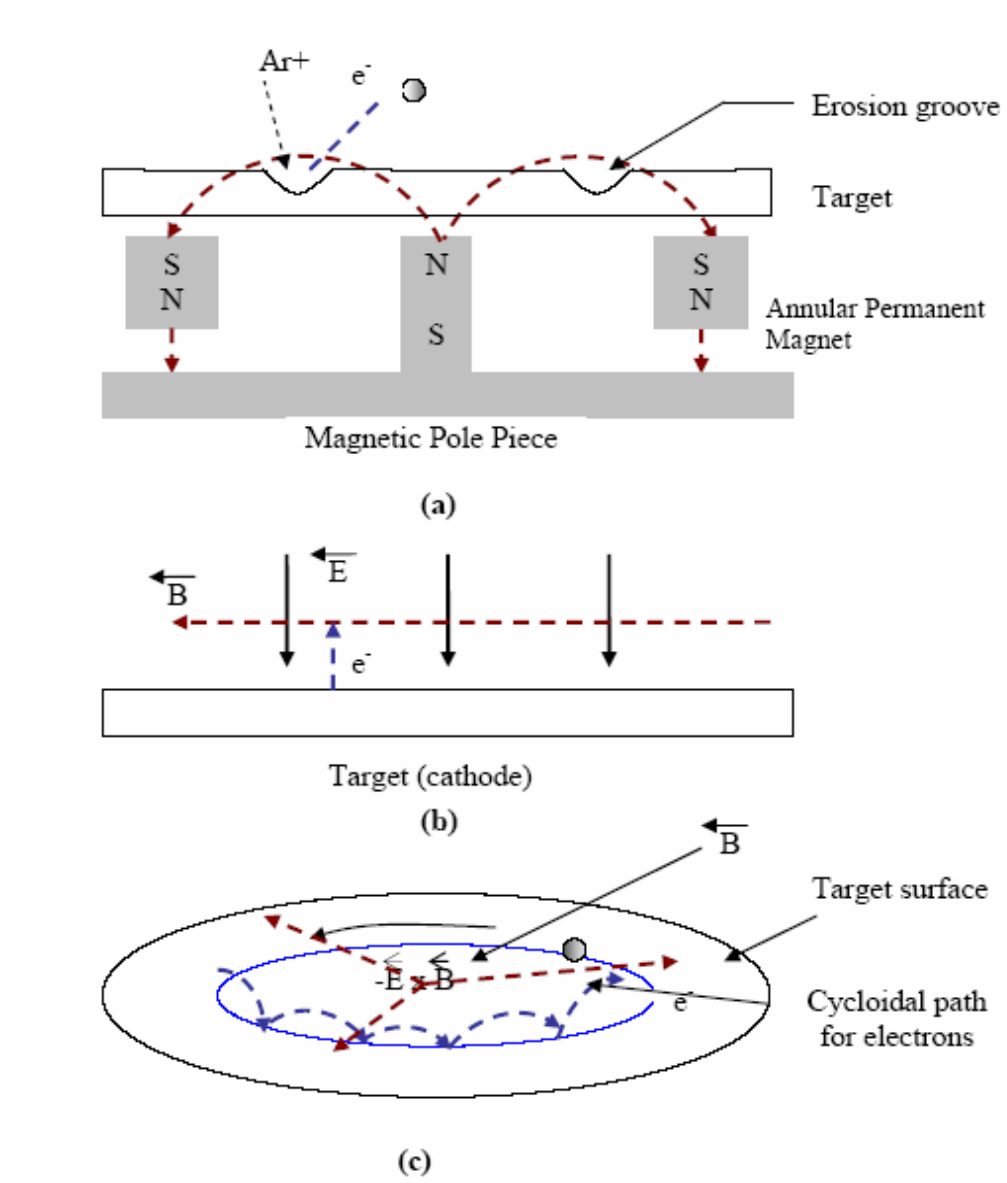

Figure 3.1: The Planar Magnetron Arrangement (a) Cross-sectional view of the annular design of of the magnetron and as a result of which an erosion groove is formed on the surface of the target. (b) For both DC and RF sputtering, a static magnetic flux is created perpendicular to the electric field (c) The electrons drift in the the -E x B direction executing a cycloidal path.

For the most common magnet arrangement, the resulting shape of plasma is torroidal. This is due to the fact that ring of magnets confines the electrons in to an annular closed path, which in turn produces an annulus of intensified sputtering plasma. This results in a donut shaped erosion pattern on the target with only about 30% of the target being used. One way to increase target material utilization is to move the target with respect to magnets (swept field magnetron) during deposition. Other methods involve departing from the planar geometry and changing the shape of the target and/or arrangement of the magnets so that the plasma bombards the target more uniformly over its entire surface.

An alternative to sputtering deposition techniques described above is ion beam sputtering. In this technique, a low voltage discharge is established within an ion source. The entire source is biased to a high DC potential, on the order of 1 KV. An ion beam is extracted from this source and directed onto a sputtering target, possessing a maximum kinetic energy equal to the DC bias of the source.

3.1.3 Substrate Preparation

Silicon substrates were used for the experiments. The Si substrate used was p-type Si (100) wafer with the sheet resistivity in the range of 2-20Ω.cm. In order to remove the native oxide layer on top of the Si wafer, chemical etching was done for some of the Si (100) wafers by immerging the wafer in a 9:1 buffered oxide etch solution for 30 seconds.

Contaminants present at the surface of the silicon wafers at the start of processing, or accumulated during processing have to be removed at specific processing steps in order to obtain high performance and high reliability semiconductor devices and to prevent contamination of

semiconductor equipment. SC1 and SC2 cleaning (modified RCA cleaning) was used to remove organic, ionic and heavy metal contaminants from the Silicon wafers.

The SC1, SC2 procedure has two major steps executed sequentially:

1. Removal of insoluble organic contaminants using 6:1:1 $H_2O/H_2O_2/NH_4OH$ solution.
2. Removal of ionic and heavy metal atomic components using a solution of 6:1:1 $H_2O/H_2O_2/HCl$ solution.

The SC1 solution was prepared by heating the solution of NH_4OH and H_2O in the ratio of 6:1 till a temperature of 75^oC. 1 part of H_2O_2 was then added to the solution just prior to immersing the Si wafers. The wafers were cleaned for 15 minutes. This was followed by a DI water rinse for 5 minutes.

For SC2, the SC2 solution was prepared by heating the HCl and H_2O in the ratio 6:1 to 75^oC. H_2O_2 was added just prior to immersing the SC1 cleaned wafers in the solution. A 15 minutes SC2 clean was followed by 5 minutes DI rinse, after which the wafers were blown dry using a N_2 gun.

3.2 Sample Characterization

Detailed surface morphology of the films was characterized using Digital Instruments Atomic Force Microscope (Nanoscope Dimension 3100 series scanning probe microscope). Mechanical behavior of the deposited SiCN films was evaluated using a Hysitron TriboScope by carrying out nano-indentation tests. The Hysitron TriboScope is a high-resolution nano-mechanical test instrument capable of performing both indentation and scratch testing. When mounted to an Atomic Force Microscope, it can also provide in situ images.

A Berkovich (3-faced pyramid) diamond tip using a single loading-unloading cycle made the indentations. Indentations were performed at various locations across the wafer with loads ranging from 60 up to 1800 μN. Multiple indentations were made in order to confirm the accuracy and repeatability of testing results. The indenter tip shape had been calibrated following the procedure described by Oliver and Pharr [33] and a quartz standard were used to check the calibration of hardness measurement. The upper part of the loading curve was fit by a power law to determine the hardness and Young's modulus [33].

The silicon carbide nitride thin films were also characterized using 5400 PHI ESCA (XPS) spectrometer at the base pressure of 10^{-9} Torr using Mg Kα X-radiation (1253.6eV) with a power of 350 W. Survey and individual high resolution spectra were recorded with a pass energy of 44 and 17 eV to achieve the maximum instrument resolution. The binding energy (BE) of gold ($4f_{7/2}$) line at 84 ± 0.2 eV was used to calibrate the binding energy scale of the spectrometer. Survey scans (44.75 eV pass energy, 0.5 eV step) were obtained in the BE range between 0 and 1100 eV. Survey scans were collected first to confirm the presence of N, C, and Si, and to select peaks for deconvolution. Individual high resolution scans were then collected of the N1s, C1s, and Si2p peaks so that the effect of nitrogen co-sputtering could be studied. A similar procedure was adopted to study the oxidation kinetics for the films after annealing in dry oxygen ambient in the temperature range of 400°C to 900°C. In addition to the N1s, C1s and Si2p peaks, high resolution scans of the O1s peak were also collected. The high resolution scans were collected with a 0.05eV step resolution. Spectral deconvolution was performed using standard curve-fitting software. Peaks were successfully fit using Gaussian-Lorentzian component peaks located at acceptable binding energies.

The surface roughness of the oxygen annealed samples was examined by 'Veeco' optical profilometer. The effect of composition and annealing temperature was studied as a function of surface roughness. The following sub-sections will describe a brief overview of the four characterization techniques used in this thesis work.

3.2.1 Nano-indentation Characterization

The hardness of a material is defined as its resistance to local plastic deformation and can be determined by nano-indentation, in which the point of a pyramidal stylus is pressed onto the surface with a specified force.

The Hysitron TriboScope is a high-resolution nano-mechanical test instrument capable of performing both indentation and scratch testing. When mounted to an Atomic Force Microscope, it can also provide in situ images. In indentation, the instrument is a load-controlled displacement-sensing device. An indenter tip is driven into a sample and then withdrawn by decreasing the applied force. The applied load (P) and depth of penetration (h) into the sample are continuously monitored. A load v_s. depth curve can then be generated from the collected data. Fig. 3.2 depicts an example of a load vs. depth curve in which the load is increased at a constant rate to some peak value (loading), held at that value for a set amount of time and then decreased to zero (unloading) at the same rate as loading. The sample hardness (H) and reduced elastic modulus (E_r) can then be calculated from the following curve. The reduced modulus is defined by the following equation,

$$E_r = S\frac{\sqrt{\Pi}}{2\sqrt{A}}$$

Where S is the unloading stiffness $\left(\frac{dP}{dt}\right)$ and A is the projection contact area.

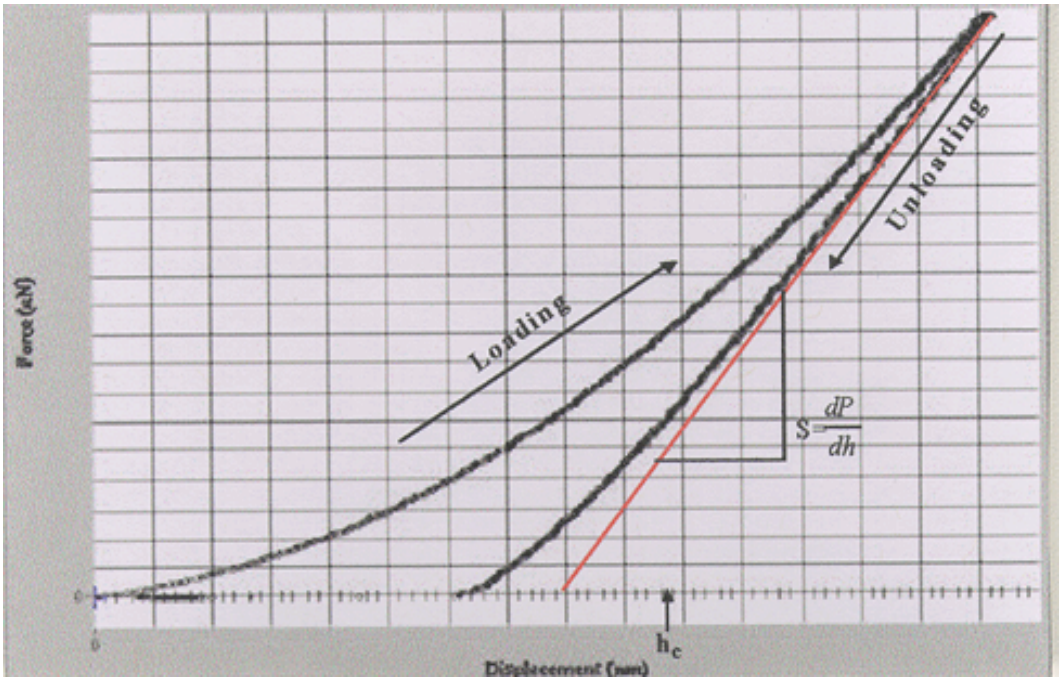

Figure 3.2: Example of a load v_s. depth curve in fused quartz.

The reduced modulus is related to the modulus of elasticity (E) through the following equation,

$$\frac{1}{Er} = \frac{(1-v_1^{\,2})}{E_1} + \frac{(1-v_2^{\,2})}{E_2}$$

Where the subscript 1 corresponds to the indenter material, the subscript 2 refers to the indented material, and v is Poisson's ratio. For a diamond indenter tip, E_1 is 1140 Gpa and V_1 is 0.07. Poisson's ratio varies between 0 and ½ for most materials.

The unloading stiffness (S) is calculated by fitting the unloading curve to the power relation, $P = A(h-h_f)^m$, where A, h, and m are arbitrary fitting parameters. The stiffness can be calculated from the derivative of the preceding equation;

$$S = \frac{dP}{dh}(h_{max}) = mA(h_{max} - h_f)^{m-1}$$

The hardness is defined by the ratio of the maximum load to the projected contact area,

$$H = \frac{P_{max}}{A}$$

The contact area is determined from a tip calibration function $A(h_c)$ where h_c, the contact depth, is found by using the following equation

$$hc = h_{max} - \varepsilon \frac{p_{max}}{S}$$

To account for edge effects, the deflection of the surface at the contact perimeter is estimated by taking the geometric constant ε as 0.75. An image of the deformed surface can also be generated immediately before and after the indentation when the instrument is mounted to an AFM.

3.2.2 Atomic Force Microscopy

The AFM, developed in the late 1980's, produces a magnified image using a diamond probe having a tip so fine that it may consist of a single atom, dragged over the surface of a specimen to feel the contours of the surface. In effect, the tip acts like the stylus of a record player, reading the surface. The tiny up-and-down movements of the probe are converted to an image of the surface by computer and displayed on a screen.

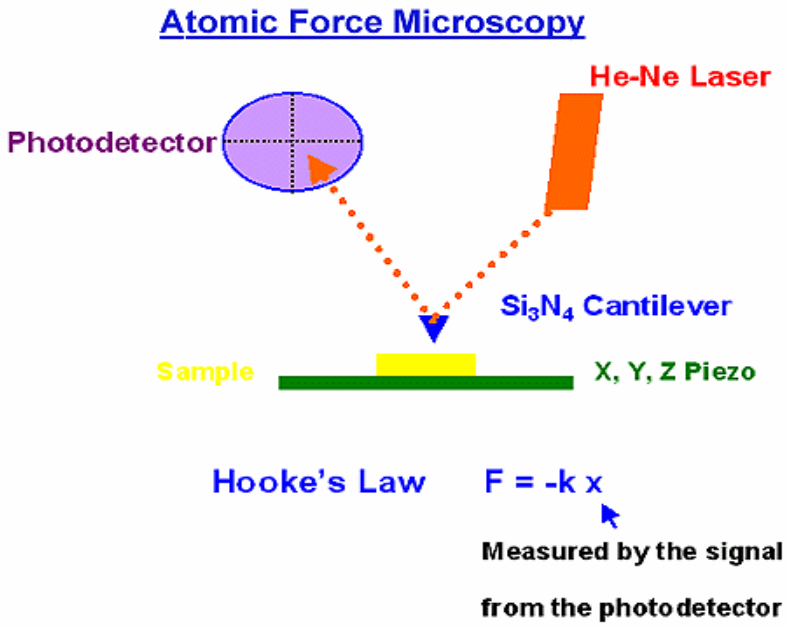

Figure 3.3: A Schematic diagram of Atomic Force Microscope experimental setup.

A laser is aimed at the reflective back of the cantilever, Fig. 3.3, and as the laser is scanned across the surface the orientation of the cantilever changes due to interactions with species on the surface of the sample.

The variations in the position of the cantilever cause a change in the angle and orientation of the reflected laser light. A photo-detector records the changes in the orientation of the laser light and sends this data to the computer. Deflections of laser light due to cantilever displacements as small as 0.001 nm can be detected. The three-dimensional topography of the sample can then be imaged from this data.

3.2.3 X-ray Photoelectron Spectroscopy

X-ray photoelectron spectroscopy (XPS, sometimes also referred to as ESCA, electron spectroscopy for chemical analysis) is a broadly applicable surface analysis technique that can detect all elements except hydrogen and helium. Samples can be gaseous, liquid, or solid, but most electron spectrometers are designed for solids. XPS can probe surfaces to a depth of 20-60Å. It can be used to analyze all kinds of samples including metallic, polymer or organic materials, since XPS is the least destructive of all the electron or ion spectroscopy techniques (soft x-rays).

XPS irradiates a sample's surface with soft x-rays, and then measures the kinetic energies of the photoelectrons emitted from the surface. The resulting spectrum is a plot of the kinetic energy versus the intensity of the detected electrons. As shown in Fig. 3.4, an incident photon strikes out a core level electron producing an ejected free electron. The kinetic energy of this ejected electron depends on the energy of the photon expressed by the Einstein's photoelectric equation.

$$KE = h\nu - BE - \phi$$

Where,

$h\nu$ = the x-ray energy

BE = binding energy of the particular electron to the atom concerned

ϕ = work function of the spectrometer

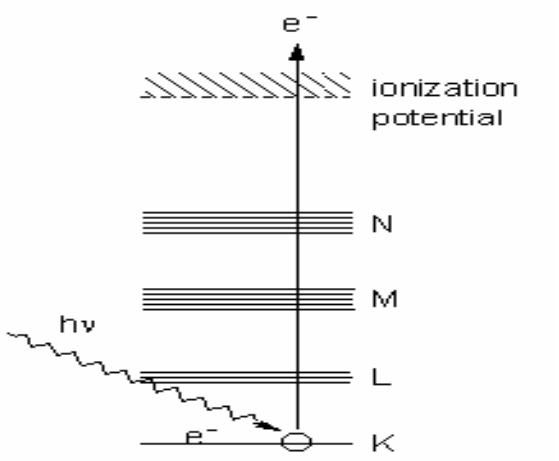

Figure 3.4: Energy level diagram for XPS.

The kinetic energies of the ejected electrons identify the elements present in the sample, since these energies are related to the binding energies (BE) of the electrons. It is also possible to identify the chemical state of the elements both from small shifts in the BE of core electrons and from larger shifts in the BE of the valence electrons participating in chemical bonding. Photoelectron intensities can be used to provide the relative concentrations of the elements present.

When the surface is bombarded by soft x-rays, we can also have the emission of Auger electrons along with photoelectrons. In this process, an outer shell electron fills the place of the ejected photoelectron. At the same time an additional electron (Auger electron) is emitted carrying the excess energy and can be considered as a measure of the kinetic energy.

3.2.3.1 Instrumental design

An XPS spectrometer usually uses either the 1486.6 eV or 1256.6 eV soft x-ray line from an Al or Mg coated anode struck by high voltage electrons. Electrons emitted from the sample travel through a series of electron lenses to the instrument's analyzer. The most popular analyzer is the hemispherical sector, which consists of two concentric hemispheres maintained at a voltage difference. As the voltages on the lenses and analyzer are varied, the trajectories of the electrons ejected from the sample at different energies are brought to a focus, in turn, at the analyzer exit slit. An electron multiplier behind the slit amplifies the electron signals.

The number of peaks in the XPS spectrum corresponds to the number of occupied electron energy levels whose BE is lower than that of the incident x-ray energy. The position of the peaks directly measures the BE of the emitted electrons, thereby identifying the atoms concerned. Electrons in XPS can travel only a short distance through solids before losing energy in collisions with atoms. Photoelectrons ejected from atoms very near the surface escape un-scattered and appear in the XPS peaks. Electrons originating from deeper have less chance of escaping un-scattered and mostly end up in the background signal. Commercial spectrometers operate in ultrahigh vacuum levels of better than 10^{-10} torr, and have fast entry load-lock systems for inserting samples, which may be as large as 300-mm wafers. The reason for the ultrahigh-vacuum design is that reactive surfaces (e.g., clean metals) contaminate rapidly in poor vacuum.

It is possible to probe surface layers of varying thickness for chemical state information. The analysis depth is proportional to the mean free path of an escaping photoelectron and the sine of the angle between the analyzer input lens axis and the surface of the sample. A small angle limits the analysis to topmost layers while a 90º angle yields information about atoms 12-15 layers down. By varying the angle, it is possible to see how surface layers change with depth.

In many applications the problem being examined is not limited just to the top 2-15 atomic layer depth attainable by XPS. In this case, some physical means of stripping away the surface layers of atoms while taking data is required. The most widely used method is argon sputtering, done inside the spectrometer while taking data. It can be used to micrometer depths, but is most effective and generally used over much shorter distance because it can be a slow process and because sputtering introduces artifacts that get worse as the sputtered depth increases. XPS, AES, and SIMS are the three dominant surface analysis techniques. XPS and AES are quite similar in depths probed, elemental analysis capabilities, and absolute sensitivity. The main XPS advantages are its more developed chemical state analysis capability, somewhat more accurate elemental analysis, and far fewer problems with induced sample damage. Neither is good at trace analysis, which is one of the strengths of SIMS.

3.2.4 Optical Profilometer

Surface roughness of the thin films is an important factor in determining their reliability. Degradation in film properties occurs when the thickness is reduced to the point that the surface roughness of the film becomes comparable the film thickness. When the RMS roughness of the film exceeds 20% of the film thickness then thin spots in the film can start to dominate the film properties. The surface profile of the deposited films was measured using a VEECO NT3300 Optical profilometer. The NT3300 is a non-contact surface profiler which was used to measure the thickness and surface roughness of the sputtered dielectric and metal films. This profilometer uses two different technologies to measure a wide variety of surface heights. Phase shifting interferometry (PSI) is reliable for smooth surfaces and small steps in which the height change

between two adjacent points is not more than 160 nm. The vertical resolution for PSI mode is 3Å for a single measurement and 1Å for multiple averaged measurements. Vertical scanning interferometry (VSI) allows measurement of rough surface profiles and steps up to few millimeters high. The vertical resolution is 3nm for a single measurement and <1nm for averaged multiple measurements.

The average roughness and peak to valley roughness was measured for oxygen annealed SiCN thin films. Average roughness (R_a) represents the two dimensional roughness averages, the arithmetic mean of the absolute values of the surface departures from the mean plane.

$$R_a = \frac{1}{MN}\sum_{j=1}^{M}\sum_{i=1}^{N}\left|Z_{ji}\right|$$

where M and N are the number of data points in the X and Y direction, respectively of the array, and Z is the surface height relative to the surface reference mean plane.

Peak to valley roughness (R_t), the maximum height of the surface, is the vertical distance between the highest (R_p) and lowest (R_v) points as calculated over the entire dataset. It is defined by

$$R_t = R_p + R_v$$

Table 3.2: Operational differences between PSI and VSI measurement

Vertical Scanning Interferometry (VSI)	**Phase Shifting Interferometry (PSI)**
Neutral Density filter for white light	Narrow bandwidth filtered light
Vertically scans- the objective actually moves through the focus	Phase-shift at a single point-the objective does not move.
Processes fringe modulation data from the intensity signal to calculate surface heights.	Processes phase shift data from the intensity signal to calculate surface heights
Primarily used to measure step heights	Primarily used to measure roughness of the films

CHAPTER FOUR: RESULTS AND DISCUSSIONS

This section is divided into three main sections; first being the characterization of the as-deposited SiCN thin films by nano-indentation, AFM and XPS. The second section describes the XPS analysis of the oxygen annealing effects on the SiC thin films in the temperature range of 400°C to 900°C. Finally section three contains the characterization of SiCN films after dry oxygen annealing in the temperature range of 400 – 900 °C, by XPS and optical profilometer.

4.1. As-deposited SiCN Thin Films

Thin films of amorphous silicon carbide nitride (a-SiC_xN_y) were deposited in a RF magnetron sputtering system using a SiC target. Films with various compositions were deposited on to silicon substrate by changing the N_2/Ar gas ratios during sputtering. The detailed experimental procedure on sample preparation and characterization was described in chapter three. The following three sub sections will provide a detailed discussion on the results obtained by Nano-indentation, Atomic Force Microscopy and X-ray Photoelectron Spectroscopy for the as-deposited SiCN samples.

4.1.1. Nano-Indentation Results

Mechanical behavior of the deposited SiCN films was evaluated using a Hysitron TriboScope by carrying out nano-indentation tests. The Hysitron TriboScope is a high-resolution nano-mechanical test instrument capable of performing both indentation and scratch testing. When mounted to an Atomic Force Microscope, it can also provide in situ images.

A Berkovich (3-faced pyramid) diamond tip using a single loading-unloading cycle made the indentations. Indentations were performed at various locations across the wafer with loads ranging from 60 up to 1800 μN. Multiple indentations were made in order to confirm the accuracy and repeatability of testing results. The indenter tip shape had been calibrated following the procedure described by Oliver and Pharr [33] and quartz standard were used to check the calibration of hardness measurement. The upper part of the loading curve was fitted by a power law to determine the hardness and Young's modulus.

The results of the indentation testing of the SiCN samples had a range from 5.8 GPa to 12.2 GPa for the hardness and 73.5 GPa to 117.8GPa for the reduced modulus. Fig. 4.1 and Fig. 4.2 illustrate the hardness and reduced modulus values of the SiCN samples, each as a function of the indentation depth. For comparison purpose, SiC without nitrogen is also shown. There is a consistency in both the hardness and the reduced modulus along the indentation depths. The scattering of the data below 20 nm is due to surface roughness effects and therefore was not used in calculating the hardness and reduced modulus numerical values. Fig. 4.1 and Fig. 4.2 indicate that there is an increasing trend within the hardness and reduced modulus values as the amount of nitrogen was increased. The hardness and reduced modulus of the SiCN films showed a maximum of 12.24 and 117.8 GPa respectively for N_2/Ar flow ratio of 0.8.

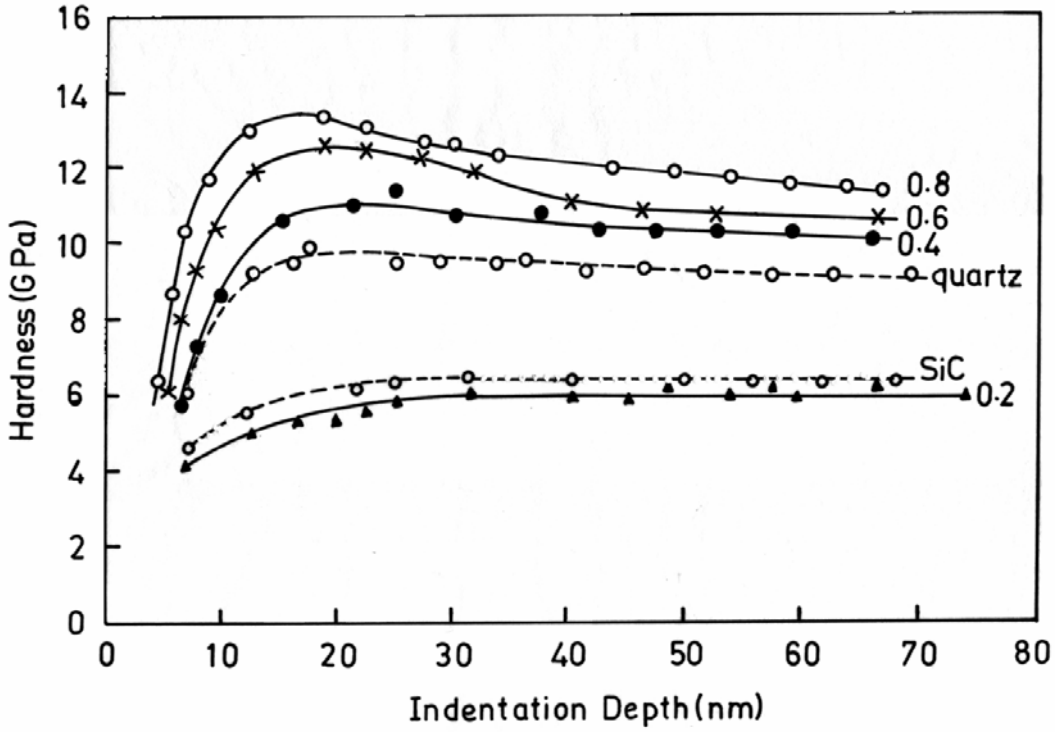

Figure 4.1: Hardness values of th SiC_xN_y films for various N_2/Ar flow ratio as function of contact depth.

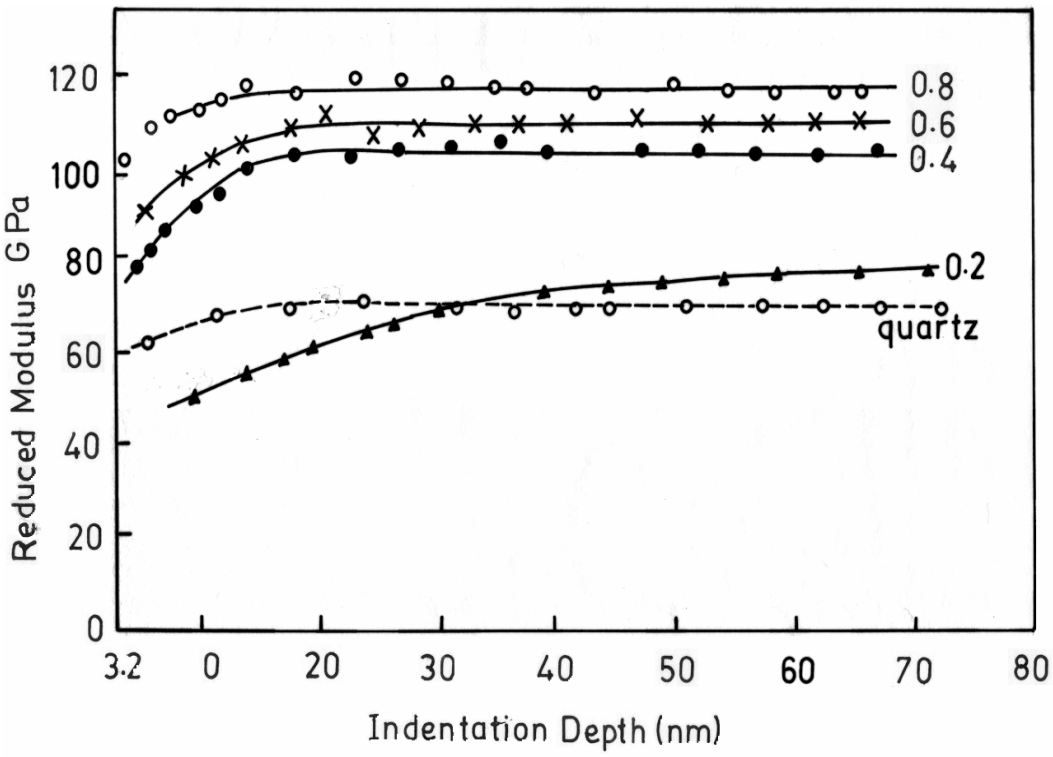

Figure 4.2: Reduced modulus values of the SiC_xN_y films for various N_2/Ar flow ratios as function of contact depth.

4.1.2. Atomic Force Microscopy Results

The film surface morphology, including grain size and shape, film voids, microcracking or lack of adhesion, and the existence of compounds are all parameters that affect the thin film properties. In the present study, detailed surface morphology of the SiC films after each oxidation step was also characterized using Digital Instruments Atomic Force Microscope (Nanoscope Dimension 3100 series scanning probe microscope).

Fig. 4.3 (a-d) show the AFM images of SiCN films deposited for N_2/Ar flow ratios of 0.2 to 0.8 respectively. AFM indicates that films grown at 0.8 N_2/Ar are much smoother than than those grown at 0.2 N_2/Ar ratio. The Fig. 4.4 shows the R.M.S. roughness as a function of N_2/Ar ratio. The R.M.S. roughness of the surface consistently decreased as the nitrogen ratio was increased during sputtering to give smoother films.. Similar increase in hardness has been reported for smoother films by Li et. al for the alumina films deposited by magnetron sputtering [34]. Hardness also improves with increasing nitrogen due to removal of voids and build of compressive stress. Smoother films seem to have less voids. Similar results were reported by Chan et. al for the nitrogenated carbon films [35].

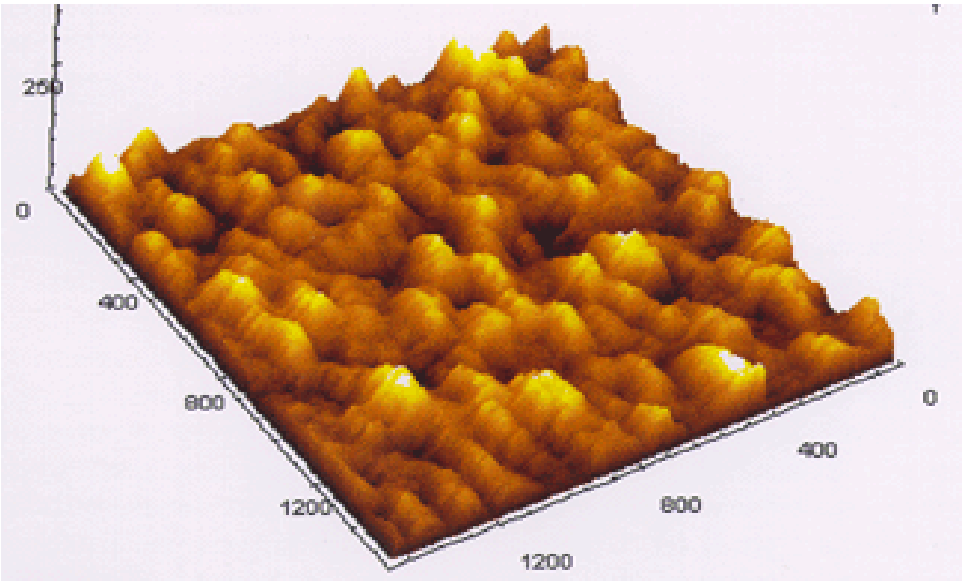

Figure 4.3 (a): AFM micrograph of SiC_xN_y film for N_2/Ar flow ratio of 0.2.

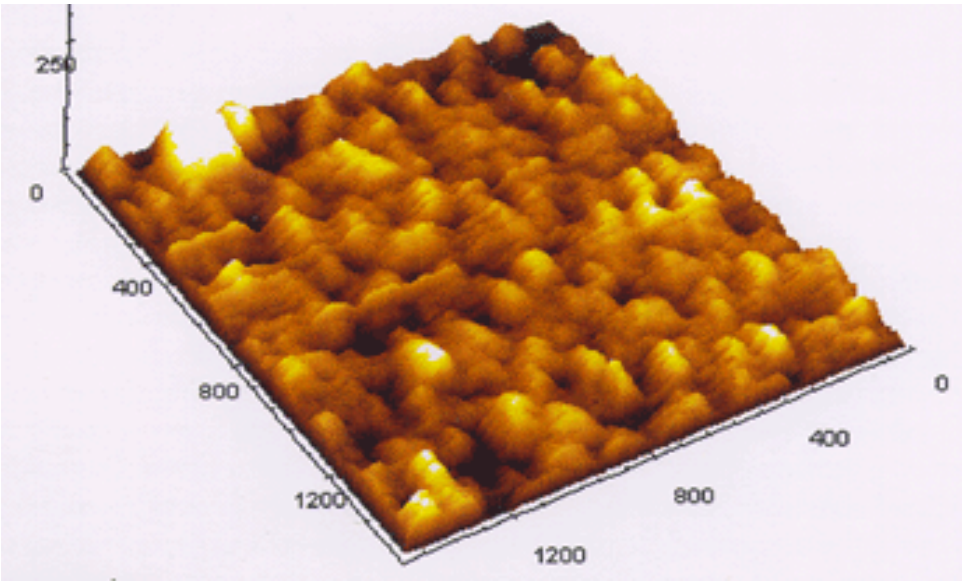

Figure 4.3 (b): AFM micrograph of SiC_xN_y film for N_2/Ar flow ratio of 0.4.

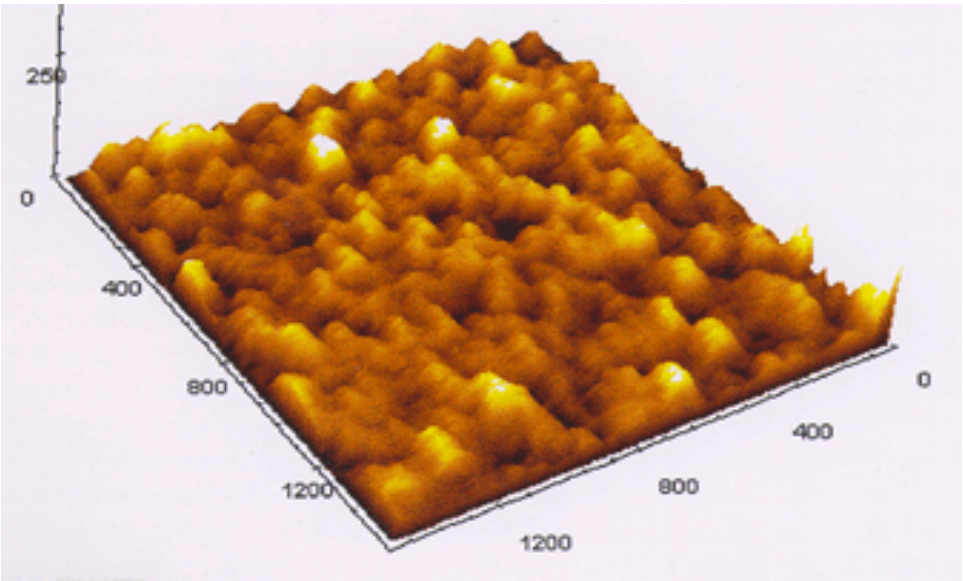

Figure 4.3 (c): AFM micrograph of SiC_xN_y film for N_2/Ar flow ratio of 0.6.

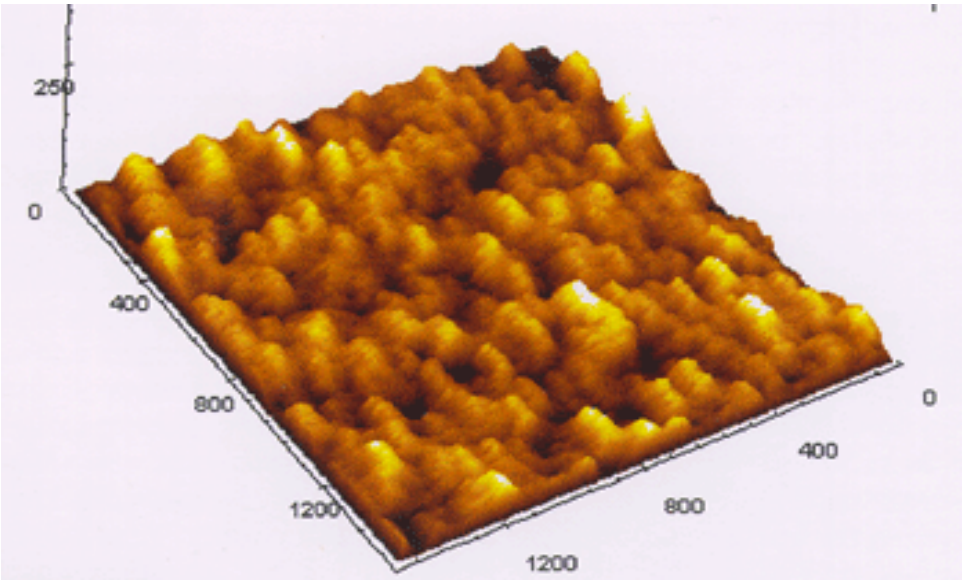

Figure 4.3 (d): AFM micrograph of SiC_xN_y film for N_2/Ar flow ratio of 0.8.

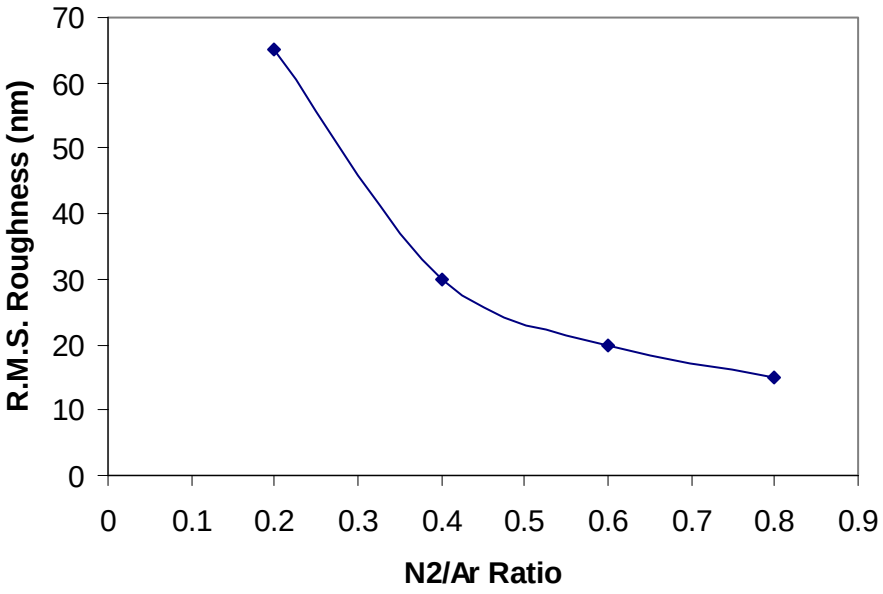

Figure 4.4: Variation of R.M.S. surface roughness as a function of N_2/Ar flow ratios for the sputter-deposited SiCN films.

4.1.3. X-ray Photoelectron Spectroscopy Results

XPS is used to analyze the incorporation of nitrogen in SiC layers grown at different N_2/Ar flow ratios (0.2 – 1.0) during sputtering. The relative atomic concentration of key elements for the films deposited at various N_2/Ar flow ratios was determined by XPS and is listed in Table 1. The most nitrogen-rich film was obtained at N_2/Ar flow ratio of 0.8, while the carbon content was lowest at this ratio. A similar trend in the decrease of nitrogen was observed during optical studies [36] where the bandgaps of the SiCN compound showed an increasing trend up to N_2/Ar ratio of 0.8. Further increase in the N_2/Ar ratio caused a decrease in the nitrogen content of our films. This decrease in nitrogen in the film may be due to the following reason. An increase in N_2 will decrease the sputtering yield compared to argon. This will reduce the probability of nitrogen reacting with sputtered SiC atoms and the film will be nitrogen deficient. The carbon loss is correlated to the chemical bonding of nitrogen with the host atoms that is the space-filling possibilities in the amorphous carbonitride networks formed by substitution of C with N in the carbide. The silicon content was roughly constant for all the film, i.e. in the range 0.23. The XPS C 1s, and N 1s spectra of the samples shown in Fig. 4.5 and Fig. 4.6 were decomposed in several components in order to identify the chemical bonds. The figures show that carbon and nitrogen have more than one bonding state.

Table 4.1: Detailed Surface atomic concentration calculated from XPS peak heights.

N_2/Ar	**C 1s**	**N 1s**	**Si 2p**
0.2	0.2	0.09	0.21
0.6	0.18	0.10	0.21
0.8	0.18	0.16	0.27
1.0	0.2	0.10	0.26

4.1.3.1 C 1s Spectra

Deconvolved XPS C 1s spectra for various N_2/Ar flow ratios are shown in Fig. 4.5. The broad envelope of C 1s peaks clearly indicates the presence of different C 1s environments. The peak located at 284.6 eV was attributed to carbon 1s binding energy for adventitious carbon. The peak located at 282.7 eV is attributed to carbon atoms with C sp^3–Si bonds [37]. Si–C is covalent and hence leads to a reduction in the C 1s binding energy. Peaks located at 285.6–286.3 and 287.9–288.7 eV are assigned to C bonded to N and C–O (contamination) bonds, respectively [38,39]. The peaks observed at 283.5–284.2 eV are assigned to Si–C–N bonds [40]. This peak increases with N_2/Ar ratio during the film deposition. All the films show the presence of C–N bonds, hence a total conversion from SiC to SiCN is not complete. Interestingly, at higher N_2/Ar, the presence of Si–C bond indicates unreacted Si–C species and is probably due to N_2 trapped in voids. However, any formation of Si_3N_4 would be evident from C 1s XPS results and hence N 1s XPS scans are carried out.

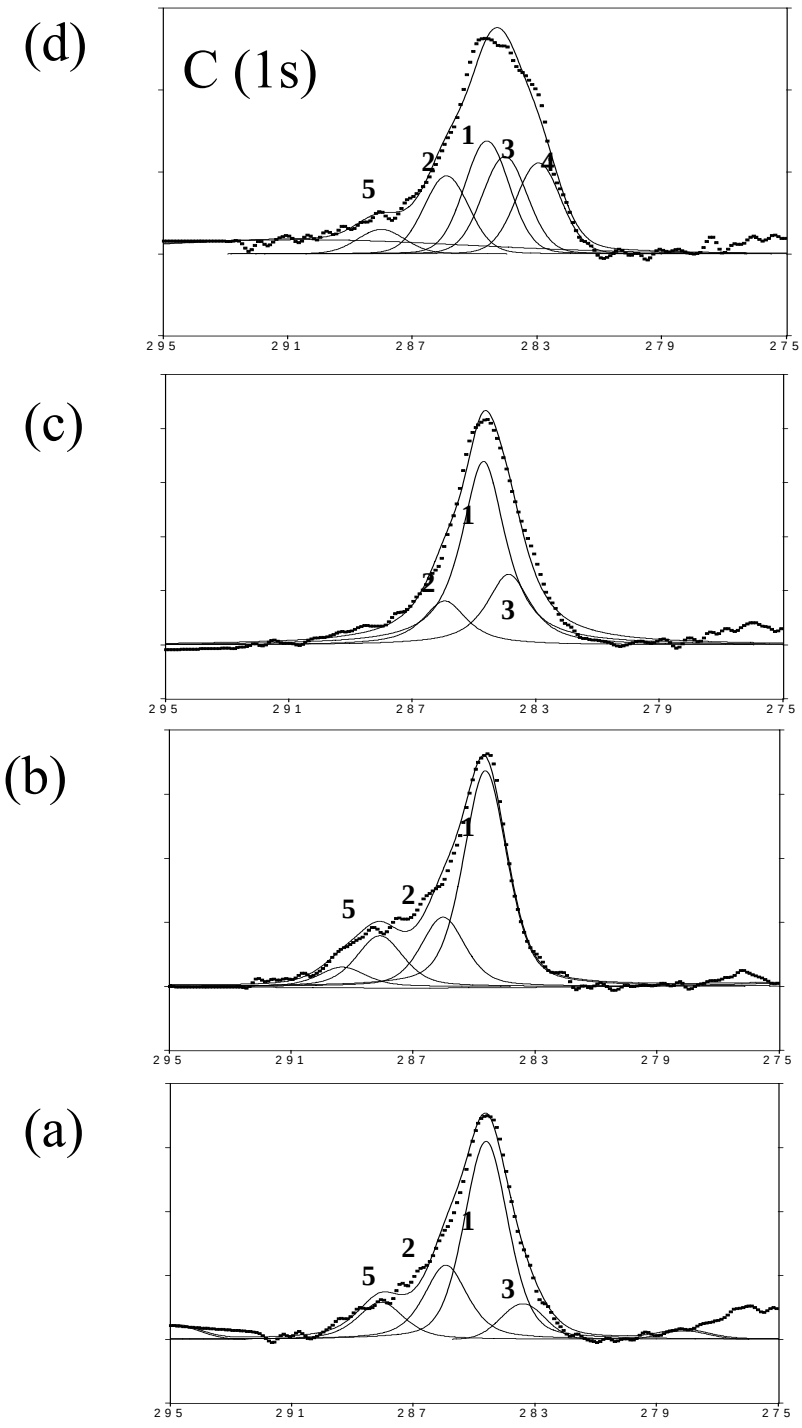

Figure 4.5: XPS C1s spectra for magnetron sputtered Si-C-N films as a function of N2/Ar ratio (a) 0.2, (b) 0.6, (c) 0.8 and (d) 1.0. Possible Peak identification: (1) CH, (2) CN, (3) SiCN, (4) SiC, (5) C=0

4.1.3.2 N 1s Spectra

The N 1s XPS spectra for films deposited at various N_2/Ar ratios shown in Fig. 4.6 indicate the presence of several N 1s states in C–N, SiCN, and Si_3N_4. Components located at 397.7–398.6, 399.4–399.8 and 401 eV were used for identification of the above compounds. The N 1s states corresponding to 397.7–398.6 eV are attributed to Si–N bonds in Si_3N_4 [41]. N 1s states corresponding to 399.4–399.8 eV are attributed to a C–N covalent bond [42, 43]. The peak at 398.2 eV is an indication of Si–C–N bond formation and the concentration increases with N_2/Ar ratios, being the highest at N_2/Ar of 0.8. Although Si_3N_4 is present for N_2/Ar ratios of 0.2 and 0.6, at higher N_2/Ar ratios, the film mostly contains Si–C–N and unreacted C–N species.

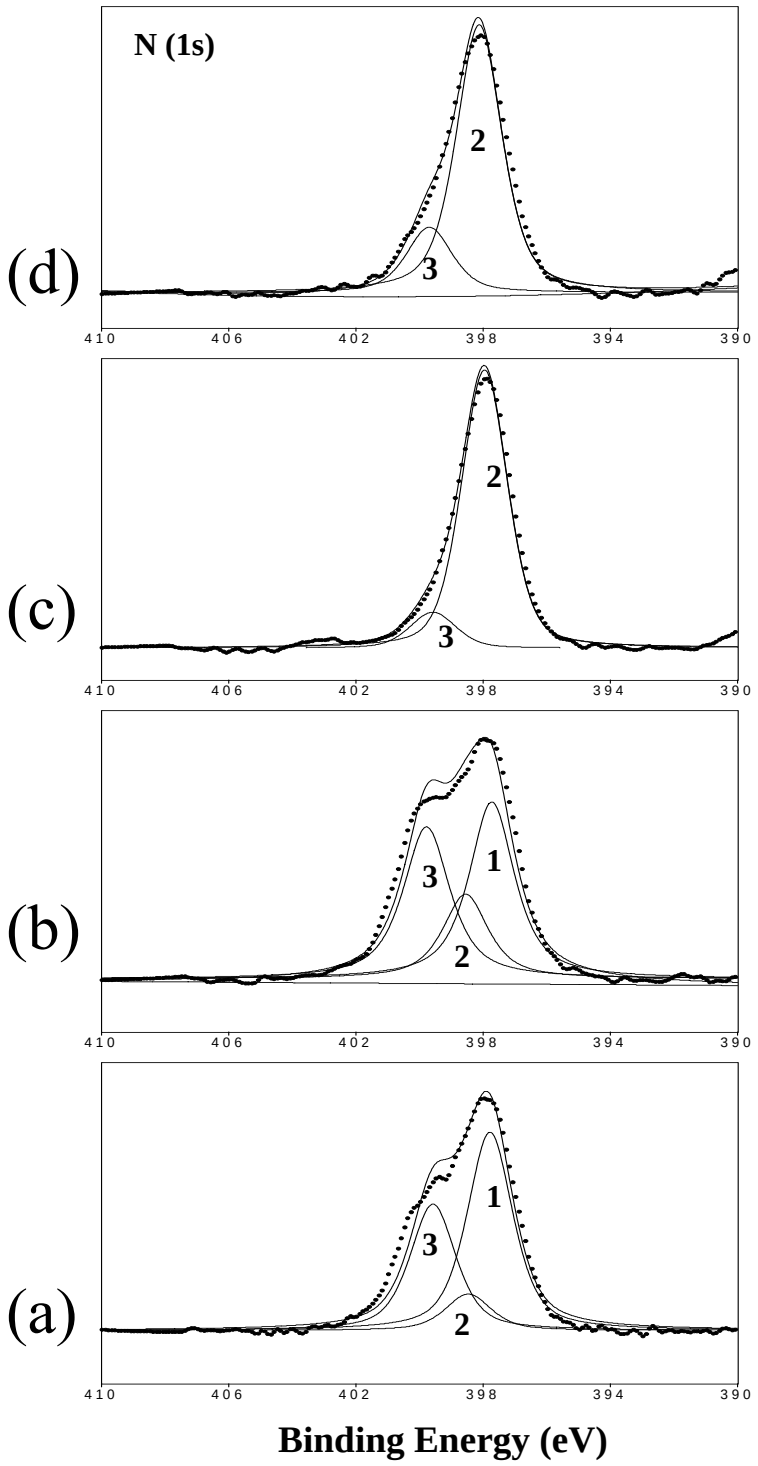

Figure 4.6: XPS N1s spectra for magnetron sputtered Si-C-N films as a function of N2/Ar ratio (a) 0.2, (b) 0.6, (c) 0.8 and (d) 1.0. Possible Peak identification: (1) Si3N4, (2) SiCN, (3) CN

4.1.3.3 Si 2p Spectra

A representative Si 2p XPS spectrum for the film deposited at N_2/Ar ratio of 0.8 is shown in Fig. 4.7. The peak shows asymmetry in the right side indicating additional presence of Si compounds. After deconvolution, the main peak at 102.3 eV is Si–C–N, where another small fraction of Si_3N_4 is present at 101.4 eV which, however, was not evident for N 1s line.

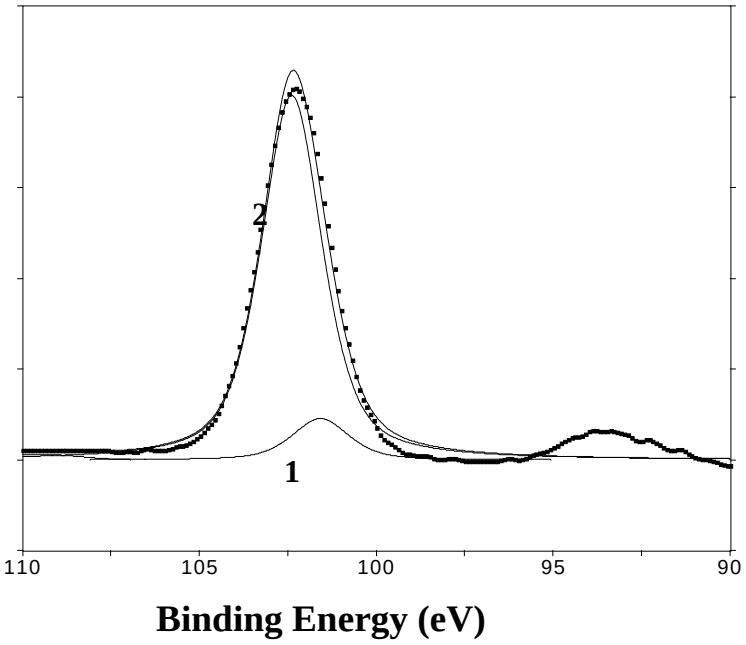

Figure 4.7: XPS Si 2p spectra for magnetron sputtered Si-C-N films as a function of N_2/Ar ratio at 0.8. Possible Peak identification: (1) Si_3N_4, (2) SiCN

4.2 Oxygen Annealing of SiC Thin Film

Amorphous silicon carbide films were deposited by RF sputtering technique using a SiC target. These films were annealed in dry oxygen ambient in the temperature range of 400-700°C. Subsequently the films were characterized using XPS to investigate the chemical composition at each annealing temperature. XPS indicated that increasing the anneal temperature results in a decrease in SiC phase, and an increase in SiO_x. The following section provides a detailed description of the important results obtained form this experiment.

4.2.1. X-ray Photoelectron Spectroscopy Results

The surface level spectra of Si2p, C1s, and O1s were taken for un-annealed SiC and for annealed samples. The O1 spectra for as deposited films and oxygen-annealed films showed a single, symmetric peak within the range of 532.0-533.0eV. The peaks may represent the bridging oxygen or the mixture of bridging oxygen and silicon-oxycarbide [44]. The following subsection describes the results of the de-convolved XPS peaks for Si2p and C1s.

4.2.1.1 Si2p Spectra

Fig. 4.8 shows the de-convoluted XPS peaks for Si2p. Fig. 4.8(a) shows a spectrum for an as deposited film. The film has strong SiC peak, at 100.7eV [45] with a FWHM of 1.6eV. Elemental Si is detected at 99.5eV [46]. The SiO peak is identified at 101.7eV [46] with a FWHM of 1.6eV. The spectra of films annealed at 400°C, 600°C and 700°C are shown in Figs. 4.8(b) through 4.8(d) respectively.

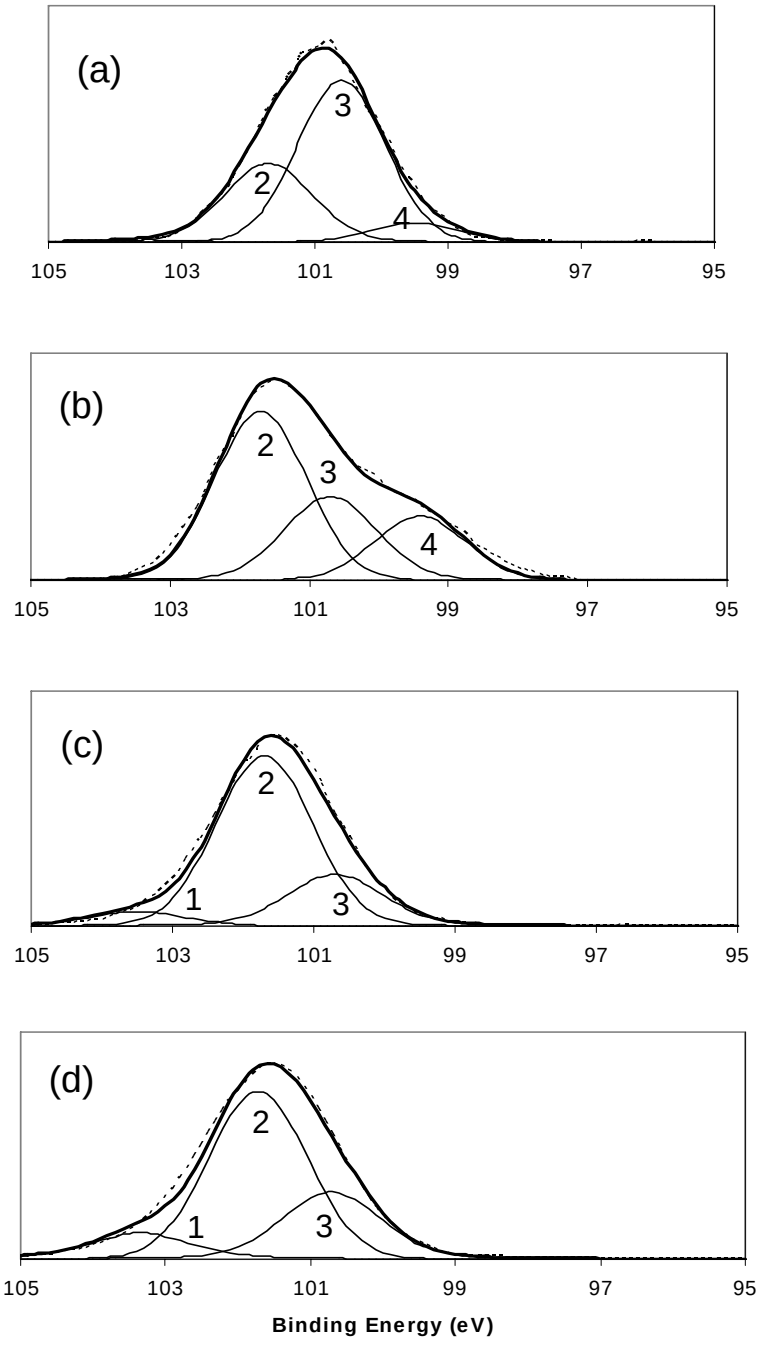

Figure 4.8: Deconvoluted XPS spectra for Si2p; (a) as deposited; (b) annealed at 400°C; (c) annealed at 600°C; (d) annealed at 700°C. Possible peaks identified (1) SiO_2 -103.5eV; (2) SiO - 101.7eV; (3) SiC - 100.7eV; (4) Si - 99.5eV.

The SiC peak decreases in intensity with increasing annealing temperatures, while the SiO_x increases with annealing temperatures. Hence, increasing the annealing temperatures causes the Si to oxidize to form SiO and SiO_2. Traces of SiO_2 were first seen for samples annealed at 600°C as shown in Fig. 4.8(c). The SiO_2 peak was identified at 103.5eV [45, 46] with a FWHM of 1.6eV. The SiO_2 peak became stronger as the annealing temperature was increased from 600°C to 700°C.

4.2.1.2 C1s Spectra

Figure 4.9(a) shows the XPS spectrum of C1s for un-annealed samples. The C1s surface level spectra of the as deposited film clearly indicated the existence of two different C1s states. The adventitious carbon was identified at 284.5eV [47] with a FWHM of 1.95eV. The C1s peak corresponding to C bonding to Si was identified within the range of 282.7 to 283.4 eV [47] with a FWHM of 1.95eV. The C1s spectra for samples annealed at 400°C, 600°C and 700°C are shown in Figs. 4.9(b) through 4.9(d) respectively. Increasing annealing temperature resulted in a decrease in adventitious carbon, which might be due to oxygen bonding to carbon to form CO/CO_2 which escapes as gas during annealing.

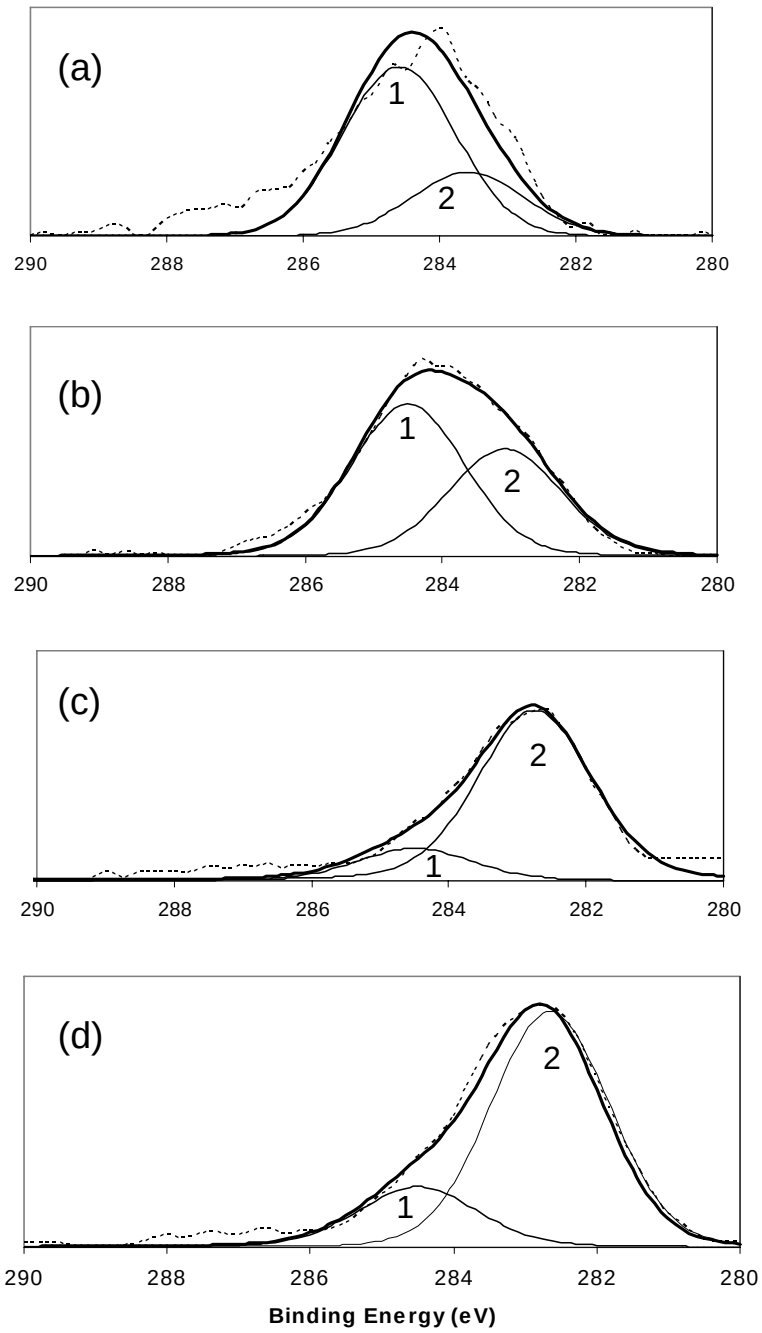

Figure 4.9: Deconvoluted XPS spectra for C1s; (a) as deposited; (b) annealed at 400°C; (c) annealed at 600°C; (d) annealed at 700°C. Possible peaks identified (1) C1s - 284.5eV; (2) C-Si 283.4-282.5eV.

4.3 Oxygen Annealing of SiCN Thin Film

Thin films of amorphous silicon carbide nitride (a-SiC_xN_y) were deposited in a RF magnetron sputtering system using a powder pressed SiC target. Films with various compositions were deposited on to silicon substrate by changing the N_2/Ar gas ratios during sputtering. These films were annealed in dry oxygen ambient in the temperature range of 400-900°C. Subsequently these annealed films were characterized using X-ray photoelectron spectroscopy (XPS) to investigate the chemical composition and oxidation kinetics at each annealing temperature. The effect of oxygen annealing on the surface roughness was studied using optical profilometer at each annealing temperature for each composition. The following two sub-sections provide a detailed description of the results form these two characterization techniques.

4.3.1. X-ray Photoelectron Spectroscopy Results

XPS was used to study the effects of various N_2/Ar flow ratios (0.25-1) on sputter deposited SiCN thin films. The relative atomic concentrations of key elements on the film's surface are displayed in Fig. 4.10. The film is richer in N_2 when deposited with a N_2/Ar ration of 0.25. Alizadeh et. al. [48] similarly found that films richest in N_2 were deposited with intermediate N_2/Ar ratios. Discrepancies in the ratio yielding the most N_2 rich film however can be attributed to different sputtering tools, and targets being used.

The O1 spectra for both un-annealed and annealed films show a single, symmetric peak within the range of 532.0-533.0eV. The peaks may represent the bridging oxygen or the mixture of bridging oxygen and silicon-oxycarbide [49]. C and N concentrations are shown to decrease with increased annealing temperatures, while Si and O concentrations increase. This suggests that annealing leads to the formation of SiOx surface at the expense of SiCN and SiC. The broad envelopes of the C1s, N1s and Si2p peak confirms the presents of more than one bonding state for these elements. Peak de-convolutions were used to determine relative amounts of the possible chemical states of C, N, and Si.

(a)

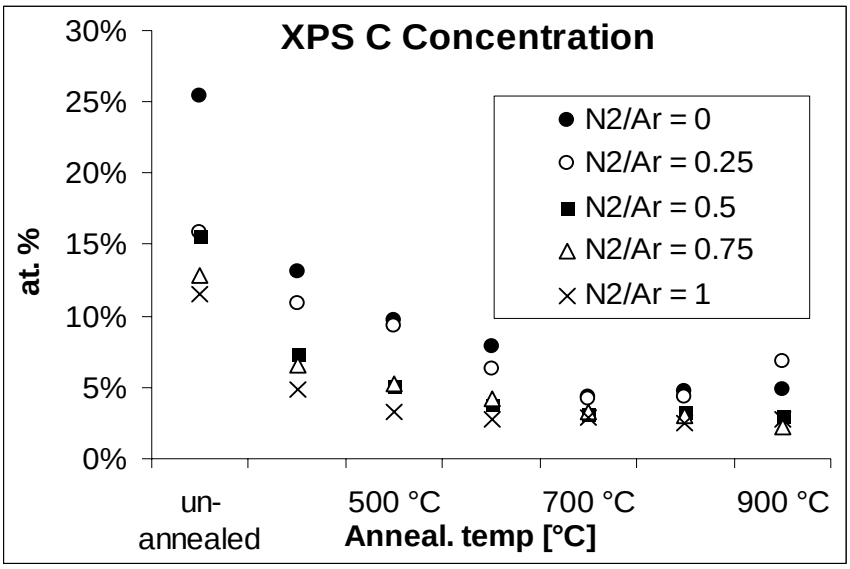

(b)

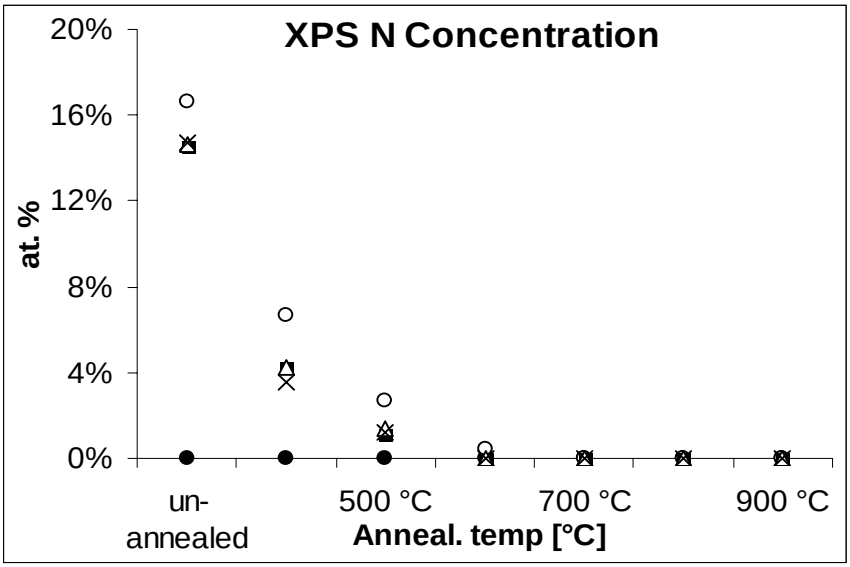
XPS N Concentration
20%
16%
12%
8%
4%
0%
at. %
un-annealed
500 °C
700 °C
900 °C
Anneal. temp [°C]

(c)

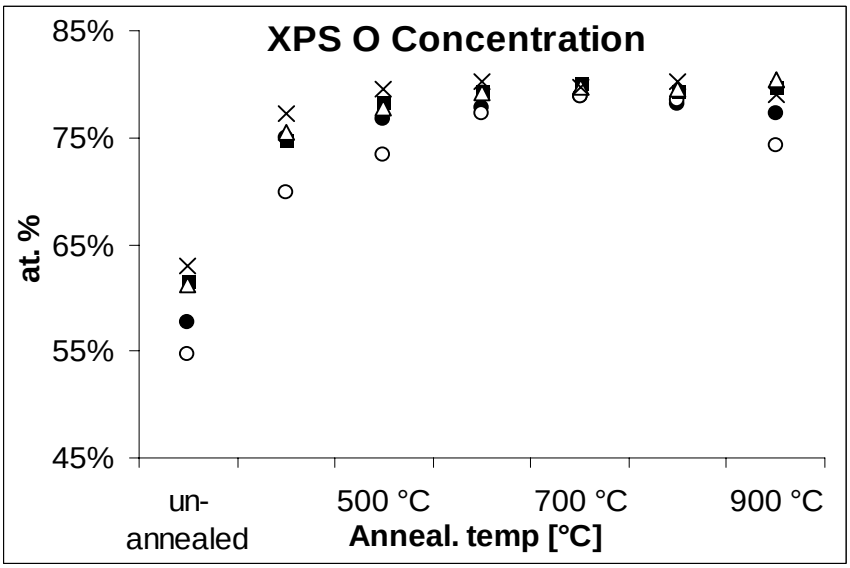
XPS O Concentration
85%
75%
65%
55%
45%
at. %
un-annealed
500 °C
700 °C
900 °C
Anneal. temp [°C]

(d)

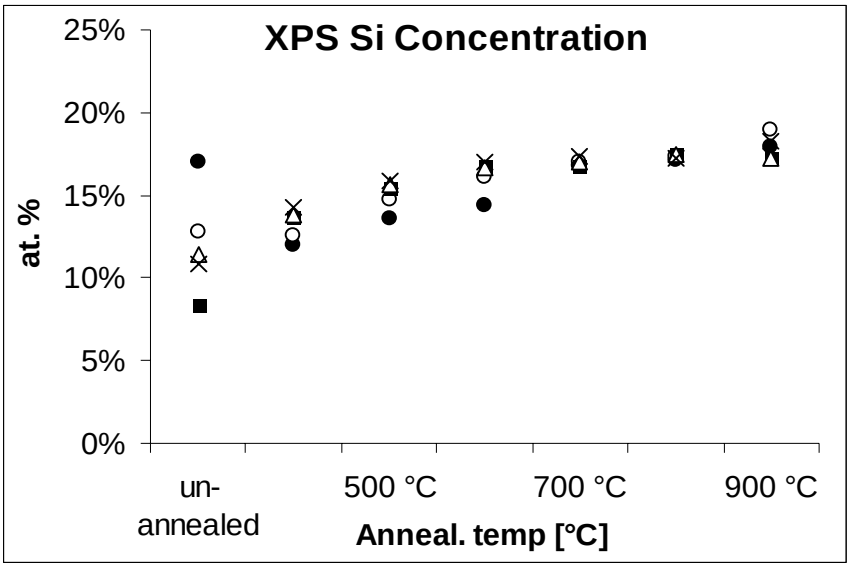

Figure 4.10: Surface atomic concentration calculated from XPS peak heights of (a) C; (b) N; (c) O; (d) Si; for various N_2/Ar rations and annealing temperatures. C and N concentrations decrease with increased annealing temperatures, while Si and O concentrations increase. Films deposited with an N_2/Ar of 0.25 are richest in N.

4.3.1.1 C1s Spectra

The C1s peak shows the effects of N_2 co-sputtering and annealing on the films surface chemistry. Adventitious carbon was located at 284.6 eV. The peak located at 282.7 eV was attributed to SiC [50]. The peak at 283.5 eV was assigned to SiCN. Peaks between 285.6-286.3 eV results from the CN (contamination) bond [51, 52]. Fig. 4.11(a) and Fig. 4.11(b) show the C1s spectra for N_2/Ar ratios of 0.25 and 1 for un-annealed specimens respectively. The concentration of SiCN increases in films deposited with higher N_2/Ar ratios. Annealing cause the breaking of SiCN bonds as shown in Fig. 4.12. Confirmation of these results was analyzed through similar analysis performed on the N1s and Si2p peaks.

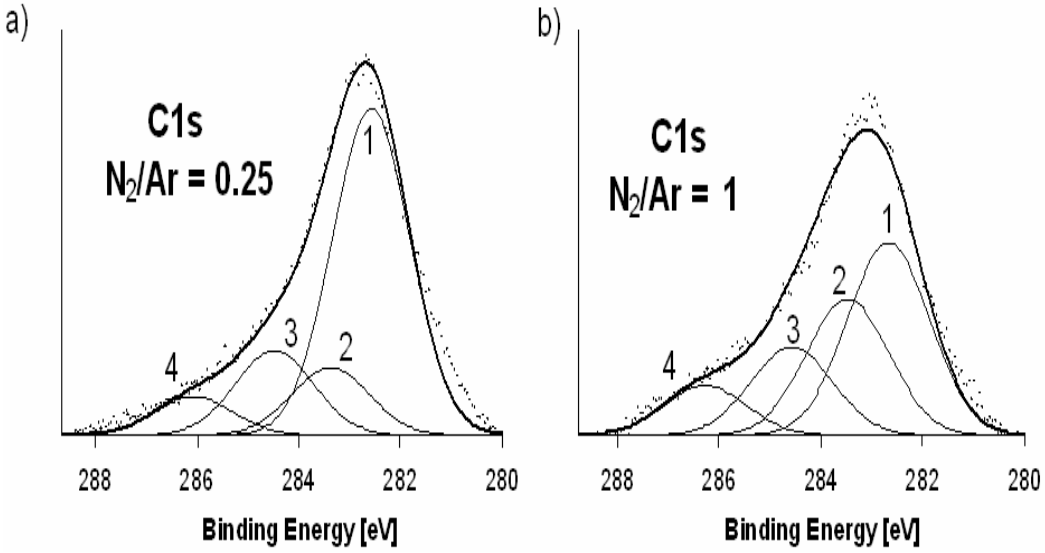

Figure 4.11: XPS C1s spectra of un-annealed Si-C-N films for N_2/Ar rations of (a) 0.25; (b) 1. Possible peak identifications: (1) SiC; (2) SiCN; (3) CH; (4) CN. SiCN increases with increasing N_2/Ar rations.

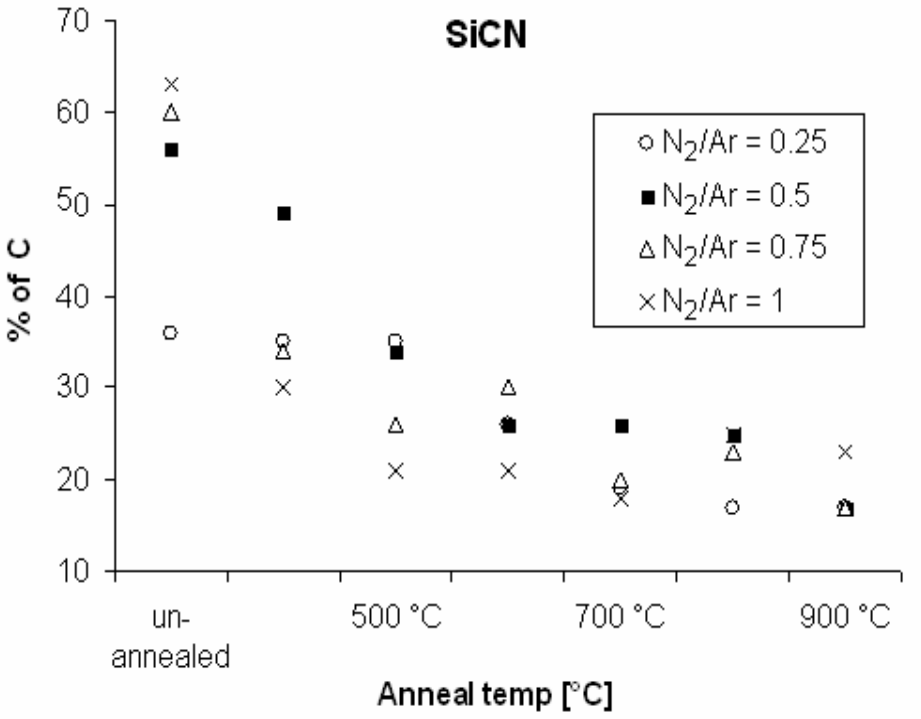

Figure 4.12: Concentration of SiCN as a function of annealing temperature, for various N_2/Ar rations. Annealing results in broken SiCN bonds.

4.3.1.2 N1s Spectra

The N1s peak shows the presence of N is several states. The peak located at 398.6 eV was assigned to Si_3N_4. The presence of SiCN results in a peak at 398.2 eV. The peak found between 399.4-399.8 eV was attributed a C-N bond. Fig. 4.13 shows the deconvoluted N1s spectra for un-annealed film deposited with N_2/Ar ratios of 0.25 and 1 respectively. An increased N_2/Ar ratio results in an increase of SiCN while the concentration of Si_3N_4 decreases, as has been previously reported. Annealing did not significantly affect the bonding state of N on the film's surface; the relative number of bonds however, is shown to decrease as shown in Fig. 4.14(a). For all N_2/Ar ratios, N concentration was found to be highest in un-annealed specimens, while the concentration approaches zero with increase in annealing temperature as shown in Fig. 4.14(b).

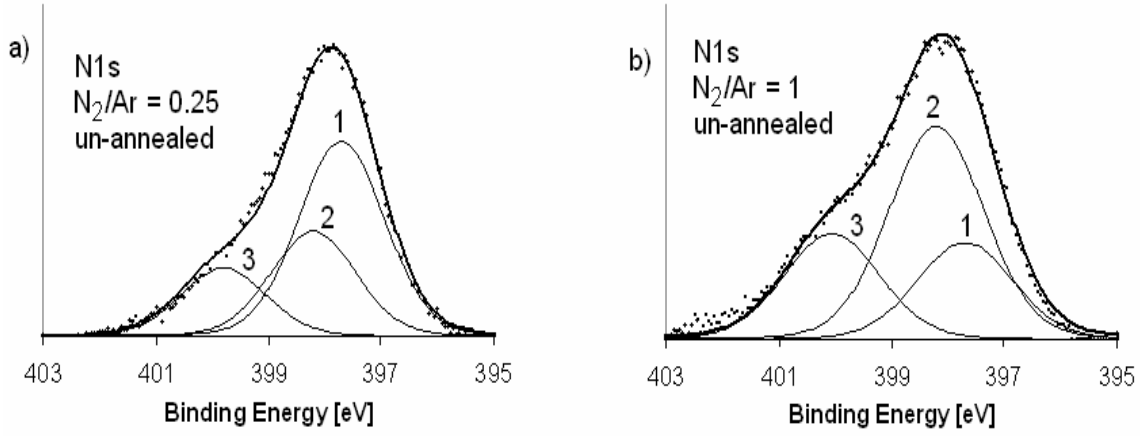

Figure 4.13: XPS N1s spectra of un-annealed Si-C-N films for N_2/Ar rations of (a) 0.25; (b) 1. Possible peak identifications: (1) Si_3N_4; (2) SiCN; (3) CN; SiCN increases with increasing N_2/Ar ratios while Si_3N_4 decreases.

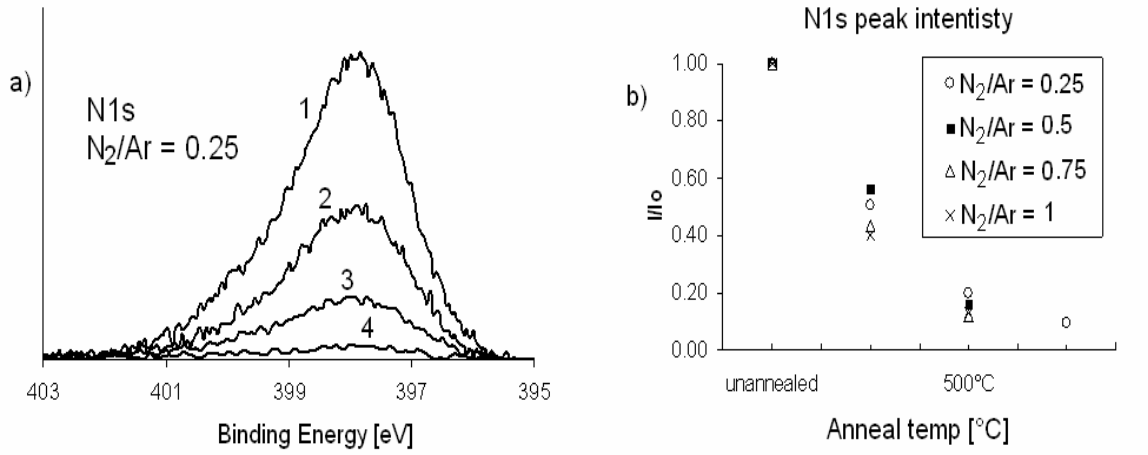

Figure 4.14: (a) XPS N1s spectra for films deposited with an N_2/Ar ratio of 0.25 at the following annealing conditions: (1) un-annealed; (2) 400°C (3) 500°C; (4) 600°C. (b) Normalized intensity ratios of the N1s peak as a function of annealing temperature for various N_2/Ar flow rates. Annealing decreases the number of N bonds on the film's surface.

4.3.1.3 Si2p Spectra

The Si2p peak of un-annealed samples was found to be broad and asymmetric, indicating several bonding states. Annealing resulted in a narrower, more symmetric peak suggesting that the various Si bonds break to form a surface oxide [53]. Peaks located at 100.7 eV were attributed to SiC [54], while SiCN yielded a peak at 102.3 eV. Peaks found at a binding energy of 101.4 eV resulted from Si_3N_4. Peaks found at 101.7 and 103.5 eV were assigned to SiO and SiO_2 respectively [55].

Fig. 4.15 shows the effect of annealing on the bonding state of Si, for different N_2/Ar ratios. The highest concentration of SiCN was found in un-annealed films, deposited with higher N_2/Ar ratios, as was suggested by deconvolving the N1s peak and the dominance of the SiC, SiCN and SiO_2 peaks made identification of Si_3N_4 difficult and inconclusive. Only films sputtered with no N_2 were seen to contain SiO_2, when not annealed.

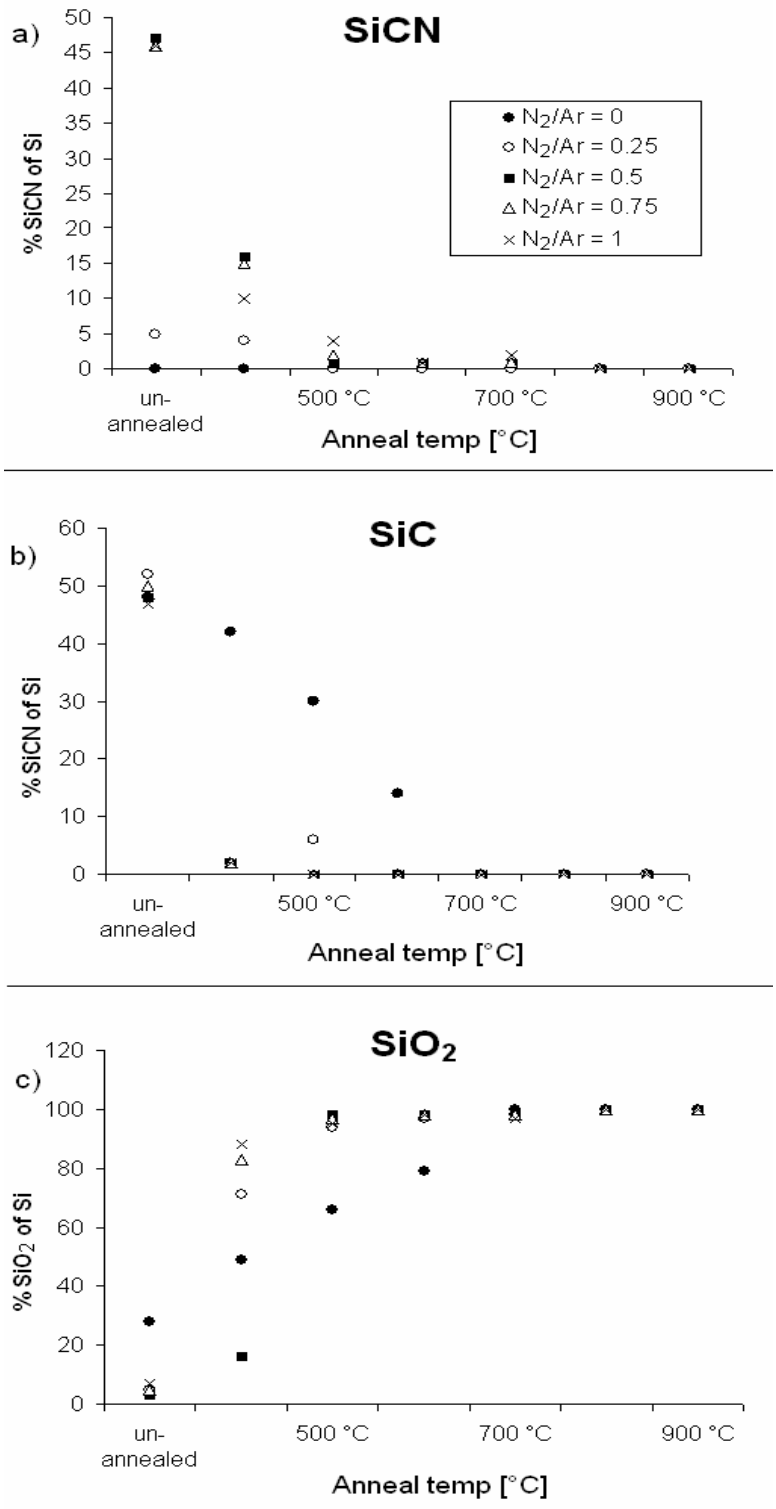

Figure 4.15: XPS concentrations of possible Si bonds: (a) SiCN; (b) SiC; (c) SiO_2; as a function of annealing temperature. The formation of a surface oxide upon annealing is evident.

4.3.2 Surface Roughness Results

The surface roughnesses of the oxygen annealed samples were examined by 'Veeco' optical profilometer. The effect of composition and annealing temperature was studied as a function of surface roughness. Four measurements were made on each sample to collect the data for roughness that includes the average roughness, the RMS roughness and the peak to valley height. Samples with 5 different compositions based on different Ar/N_2 ratios were annealed at 7 different annealing temperatures from 400°C to 1000°C, in steps of 100°C increments, to produce a total of 35 different samples. Since 4 measurements were made on each sample to improve the data quality, a total of 140 data images were captured. Only a few images are shown bellow in Fig.4.16 to 4.20.

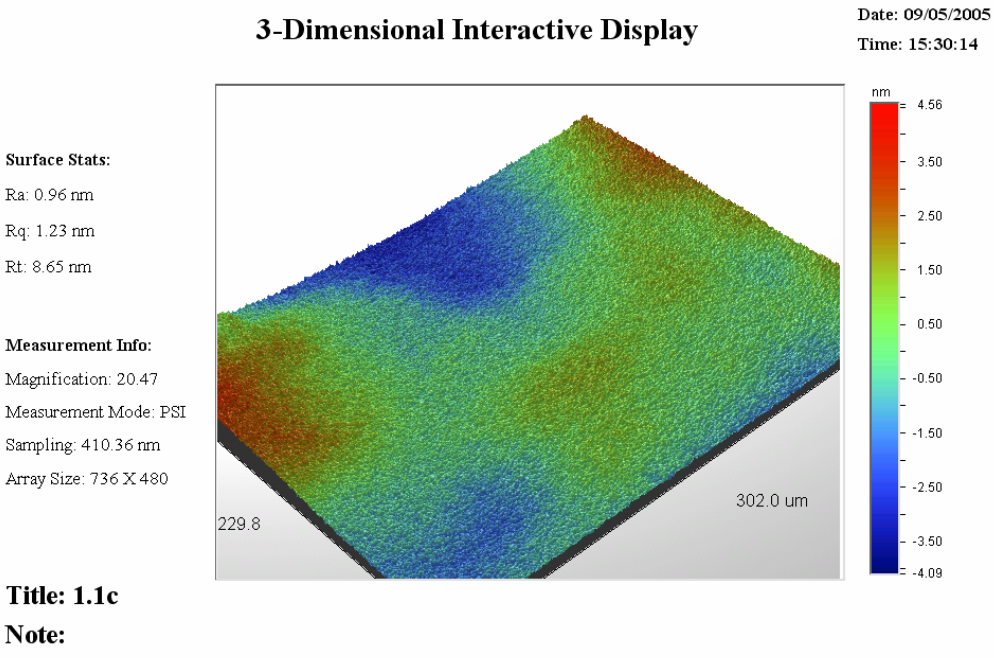

Figure 4.16: Surface roughness image for sample 1.1 taken by Veeco optical profilometer.

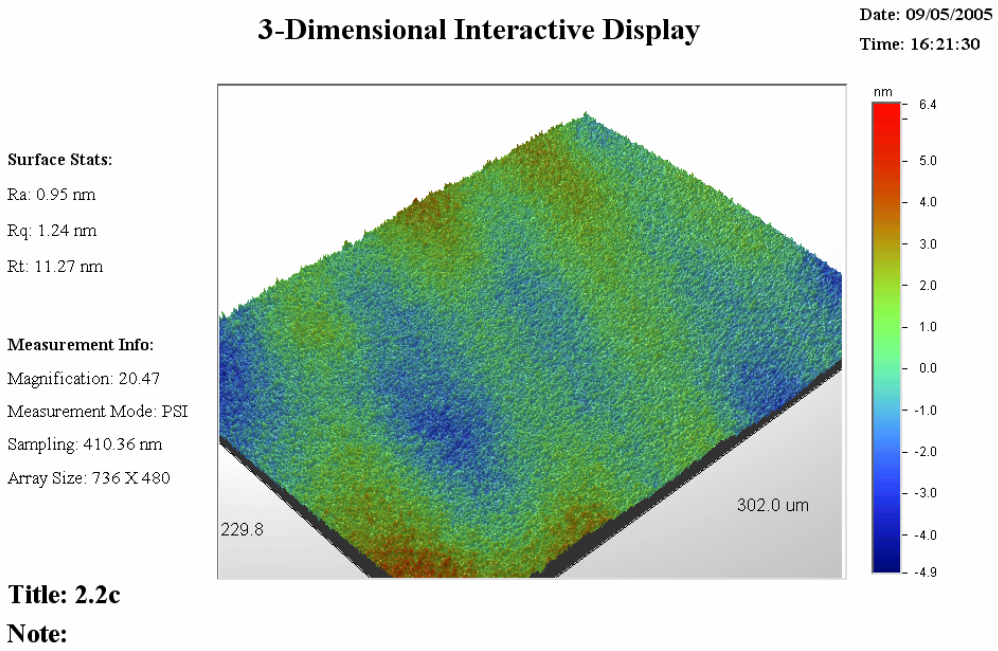

Figure 4.17: Surface roughness image for sample 2.2 taken by Veeco optical profilometer.

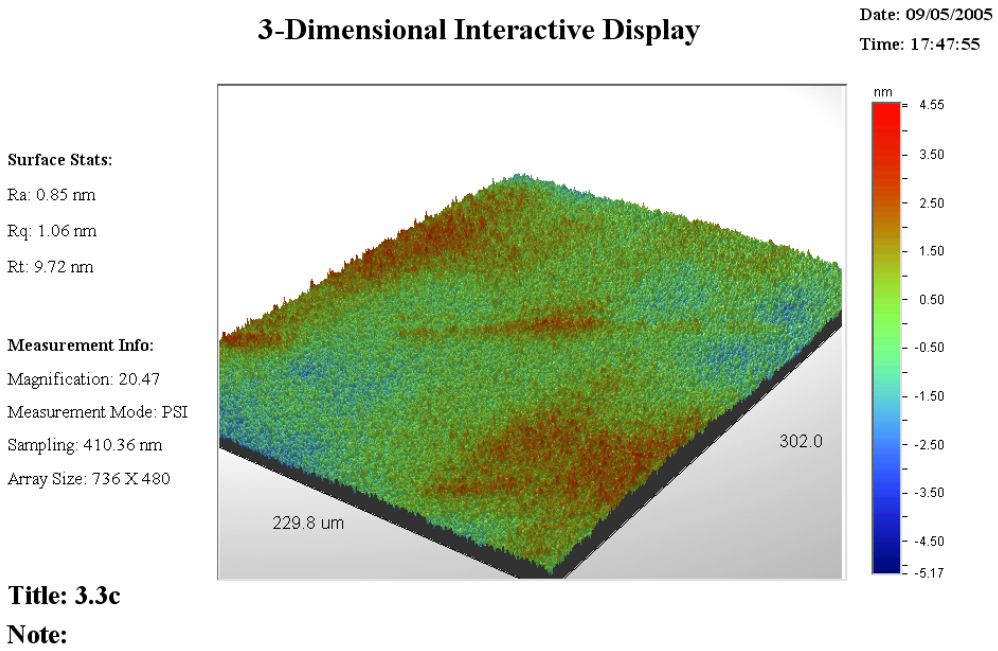

Figure 4.18: Surface roughness image for sample 3.3 taken by Veeco optical profilometer.

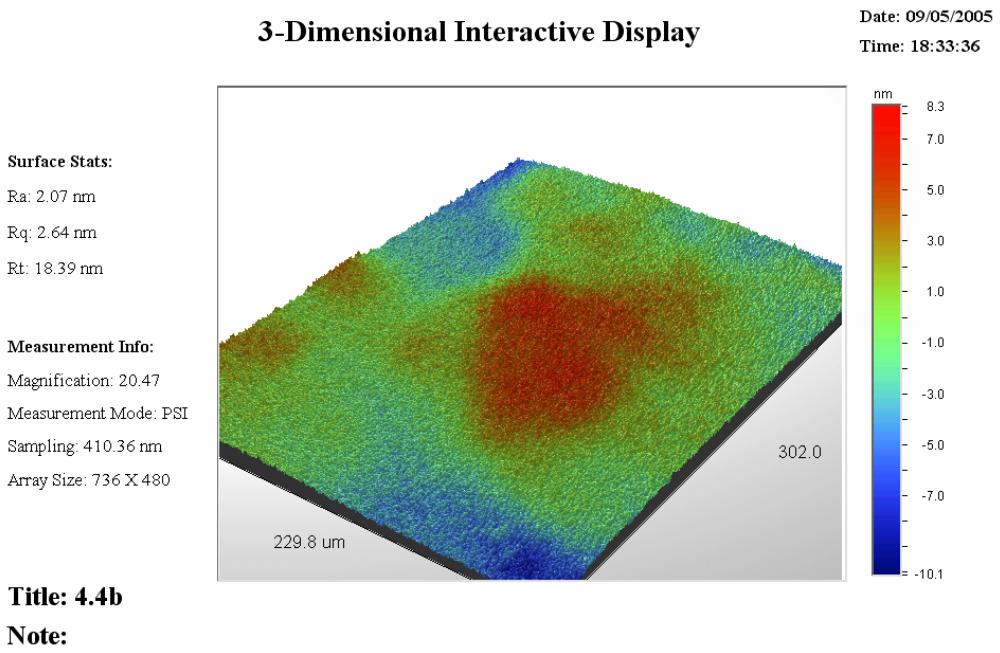

Figure 4.19: Surface roughness image for sample 4.4 taken by Veeco optical profilometer.

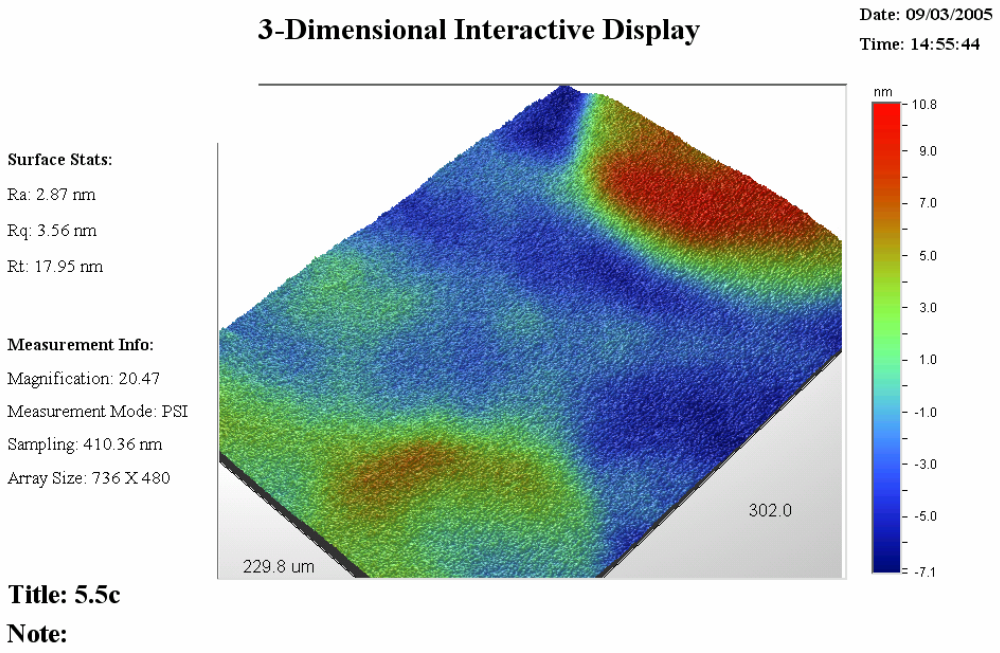

Figure 4.20: Surface roughness image for sample 5.5 taken by Veeco optical profilometer.

The data collected from these images was used to calculate the average value. The average roughness, the RMS roughness and the peak to valley height is plotted as a function of sample number that corresponds to different compositions as detailed in Table 3.1, is shown in Fig. 4.21. It is observed that samples having intermediate Ar/N_2 ratios have the best surface roughness values.

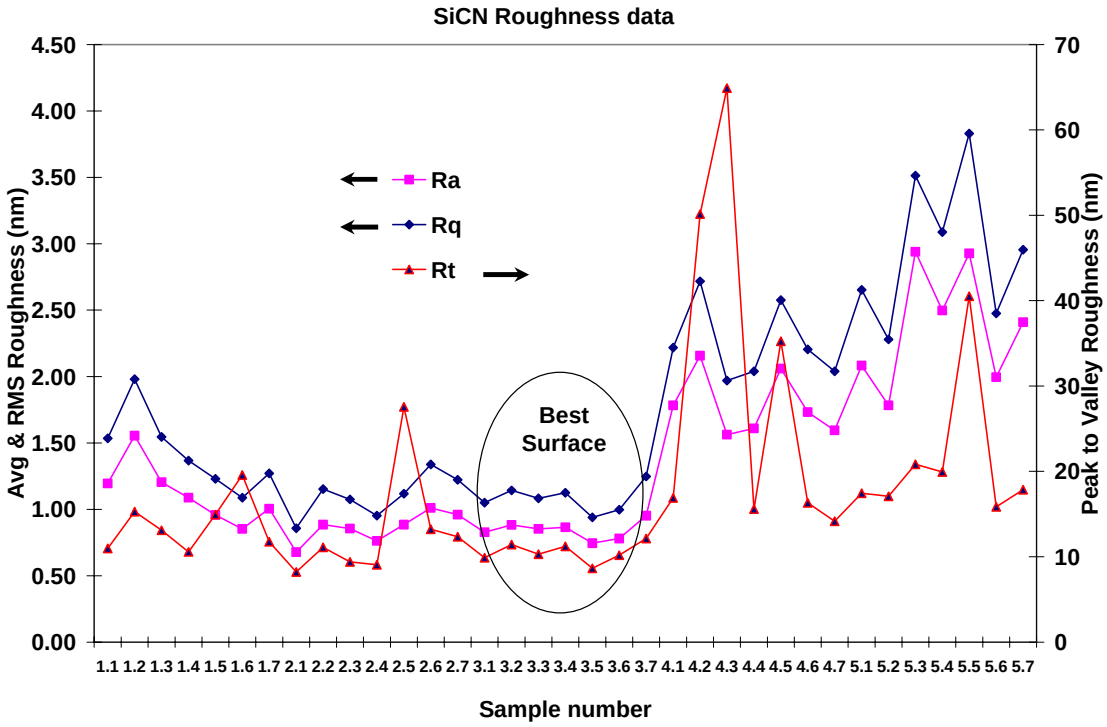

Figure 4.21: Average roughness, RMS roughness and peak to valley roughness plotted as a function of sample number that corresponds to the sample composition.

CHAPTER FIVE: CONCLUSION

Amorphous silicon carbide nitride (a-SiC_xN_y) was deposited at room temperature in a RF magnetron sputtering system using a SiC target. Nano-indentation studies were performed to investigate the mechanical properties of the SiCN films. Surface morphology was characterized by AFM. Nano-indentation studies indicated that the hardness and the reduced modulus of the films are sensitive to N_2/Ar ratios of gas flow during sputtering. AFM studies indicated that the film become smoother as the N_2/Ar ratio is increased. XPS data indicated that the chemical status is highly sensitive to the nitrogen ratios during sputtering. XPS data also indicated the existance of C-N phases in the films correlate the increase in hardness due to increased N_2/Ar ratio.

Amorphous SiC films were sputter deposited on silicon substrates and were subsequently annealed in an oxygen ambient at 400°C, 500°C, 600°C and 700°C. XPS analysis of the oxygen annealed surface of sputter deposited silicon carbide films showed and increase in SiO_x with an increase in annealing temperature. It also revealed the Si-C bonding characteristics of SiC, with the Si2p3 electron binding energy at 100.7 eV. The intensity of Si-O_2 peaks increased with increasing temperature.

Thin films of amorphous silicon carbide nitride (a-SiC_xN_y) were deposited in a RF magnetron sputtering system using a powder pressed SiC target. Films with various compositions were deposited on to silicon substrate by changing the N_2/Ar gas ratios during sputtering. These films were annealed in dry oxygen ambient in the temperature range of 400-900°C. Subsequently these annealed films were characterized using XPS to investigate the chemical composition and oxidation kinetics at each annealing temperature. The surface

roughness of the oxygen annealed samples were examined by 'Veeco' optical profilometer. The effect of composition and annealing temperature was studied as a function of surface roughness. The study of oxidation kinetics of RF sputter deposited SiCN thin films, using XPS, suggest that N_2 co-sputtering helps to suppress the formation of a surface oxide, by allowing un bonded Si to bond with N and C inside the vacuum chamber as opposed to bonding with O in atmosphere. However the bonds with N and C break readily even at low annealing temperatures. The oxidation of films was more gradual for the samples deposited with no nitrogen and hence more controllable. It was observed that samples having intermediate Ar/N_2 ratios have the best surface roughness values.

LIST OF REFERENCES

[1] S. Ulrich, T. Theel, J. Schwan and H. Ehrhardt, *Surf. Coat. Tech.*, Vol. **97**, pp 45(1997)

[2] A. Y. Liu and M. L. Cohen, *Science*, Vol. **245**, pp 841 (1989)

[3] A. Y. Liu and M. L. Cohen, *Physical Rev. B*, Vol. **45**, No. 9, pp 4579 (1992)

[4] A. Y. Liu, M. L. Cohen, *Physical Rev. B*, Vol **41**, pp 10727 (1990)

[5] V. N. Khabashesku and J. L. Margrave, *Advanced Engineering Materials*, Vol. **4**, No. 9, pp 671 (2002)

[6] F. J. Gomez, P. Prieto, E. Elizalde, and J. Piqueras, *Appl. Phys. Let.*, Vol. **69**, pp 773(1996)

[7] S. Miyagawa, S. Nakao, K. Saitoh, M. Ikeyama, H. Niwa, S. Tanemura, and K. Baba, *J. Appl. Phys.*, Vol. **78**, pp 7018 (1995)

[8] R. Capelletti, A. Miotello, and P. M. Ossi, *J. Appl. Phys.*, Vol. **81**, pp 146 (1997)

[9] A. Bendeddouche, R. Berjoan, E. Bêche, T. Merle-Mejean, S. Schamm, V. Serin, G. Taillades, A. Pradel, and R. Hillel, *J. Appl. Phys.*, Vol. **81**, pp 6147 (1997)

[10] F.J. Gomez, P. Prieto, E. Elizalde, J. Piqueras, *Appl. Phys. Lett.*, Vol. **69**, pp 773 (1996).

[11] M. Moriyama, K. Kamata, I. Tanabe, *J. Mater. Sci.*, Vol. **26**, pp 1287 (1991).

[12] G. Soto, E.C. Samano, R. Machorro, L. Cota, *J. Vac. Sci. Technol.A*, Vol. **16,** pp 1311 (1998).

[13] L. C. Chen, C.Y. Yang, D.M. Bhusari, K.H. Chen, M.C. Lin, J.C. Lin, T.J. Vhuang, *Diamond Rel. Mater.* 5 (1996) 514.

[14] W. Cheng, J. Jiang, Y. Zhang, H. Zhu and D. Shen, *Mat. Chem. Phys*, Vol. **85**, pp 370 (2004)

[15] D. Li, Y.W. Chung, S. Yang, M.S. Wong, F. Adibi, W.D. Sproul, J. Vac. Sci. Technol. A 12 (1994) 1470.

[16] K. M. Yu, M.L. Cohen, E.E. Haller, W.L. Hansen, A.Y. Liu, I.C. Wu, Phy. Rev. B 49 (1994) 5034.

[17] D. Li, X. Chu, S.C. Cheng, X.W. Lin, V.P. Dravid, Y.W. Chung, Appl. Phy. Lett. 67 (1995) 203.

[18] J. E. Lowther, M. Amkreutz, Th. Frauenheim, E. Kroke and R. Riedel, Phys. Rev. B, Vol. **68**, pp 033201 (2003)

[19] T. Tharigen, G. Lippold, V. Riede, M. Lorenz, K.J. Koivusaari, D. Lorenz, S. Mosch, P. Grau, R. Hesse, P. Streubel, R. Szargan, Thin Solid Films 348 (1999) 103.

[20] G. Lehmann, P. Hess, J.J. Wu, C.T. Wu, T.S. Wong, K.H. Chen, L.C. Chen, H.Y. Lee, Phys. Rev. B. 64, 165305.

[21] H.C. Lo, J.J. Wu, C.Y. Wen, T.S. Wong, S.T. Lin, K.H. Chen, L.C. Chen, *Diamond Rel. Mater.*, 10, pp 1916–1920 (2001).

[22] K. Yamamoto, Y. Koga, S. Fujiwara, *Diamond Rel. Mater.*, 10 (2001)

[23] M. Bruns, U. Geckle, V. Trouillet, M. Rudolphi and H. Baumann, J. Vac. Sci. Technol. A., Vol. **23**, pp 1114 (2005)

[24] H. Lutz, M. Bruns, F. Link and H. Baumann, *Surf. Coat. Tech.*, 116-119, pp 419 (1999)

[25] J. Wei, Y. Gao, D. H. Zhang, P. Hing and Z. Q. Mo, *Surface Engineering*, Vol **16**, No. 3, pp 225 (2000)

[26] K. B. Sundaram and J. Alizadeh, *Thin Solid Films*, Vol. **370**, pp 151 (2000)

[27] X. Ming He, T. N. Taylor, R. S. Lillard, K. C. Walter and M. Nastasi, *J. Phys: Condens. Matter.*, Vol. 12, pp L591 (2000)

[28] X. C. Wu, R. Q. Cai, P. X. Yan, W. M. Liu and J. Tian, *Appl. Surf. Sci.*, Vol. **185**, pp 262 (2002)

[29] E. Xie, Z. Ma, H. Lin, Z. Zhang and D. He, *Optical Materials*, Vol. **23**, pp 151 (2003)

[30] H. Misaki, M. Asano, K. Kasai, M. Fukuda and N. Imamura, IEEE Trans. Magnetics, Vol. **25**, No. 5, pp 4030 (1989)

[31] S. F. Ting, Y. K. Fang, W. T. Hsieh, Y. S. Tsair, C. N. Chang, C. S. Lin, M. C. Hsieh, H. C. Chiang and J. J. Ho, IEEE Electron Dev. Let., Vol. **23**, No. 3, pp 142 (2002)

[32] L. A. Liew, V. M. Bright, M. L. Dunn, J. W. Daily and R. Raj, The 15th IEEE International Conference on Micro Electro Mechanical Systems, pp 590 (2002)

[33] W. C. Oliver, G. M. Pharr, J. Mater. Res. **7** (1992) 1564

[34] Q. Li, Y. Yu, G. Singh Bhatia, L. D. Marks, S. C. Lee, Y. W. Chung, J. Vac. Sci. Tech. A **18** (2000) 2333

[35] W. Chan, B. Zhou, Y. W. Chung, C. S. Lee, S. T. Lee, J. Vac. Sci. & Tech. A **16** (1998) 1907

[36] K. B. Sundaram, J. Alizadeh, Thin Solid Films 370 (2000) 151

[37] A. Tabata, Y. Kuno, Y. Suzuoki, T. Mizutani, J. Phys. D 25 (1996) 194

[38] Z. Gong, E. G. Wang, G. C. Xu, Y. Chen, Thin Solid Films 348 (1999) 114

[39] R.C. Lee, C. R. Aita, N.C. Tran, J. Vac. Sci. Tech. A 9 (1991) 1351

[40] F. Ibrahim, J.I.B Wilson, p. John, A.G. Fitzgerald, A. Cook, J. Non-Cryst. Solids 175 (1994) 195

[41] Z. Gong, E. G. Wang, G. C. Xu, Y. Chen, Thin Solid Films 348 (1999) 114

[42] A. Bendeddouche, A. Berjoan, E. Beche, T. Merel-Mejean, S. Schamm, V. Serin, G. Taillades, A. Pradel, R. Hillel, J. Appl. Phys. 81 (1997) 6147

[43] Z. Gong, E. G. Wang, G. C. Xu, Y. Chen, Thin Solid Films 348 (1999) 114

[44] H. Li, S. Dimitrijev, D. Sweatman, H.B. Harrison, P. Tanner, B. Feil, J. of App. Phy. 86 (1999) 4316

[45] M.A Hartley, J.N. Chiang, D.W. Hess, D.S. Soane, Appl. Phys. Lett. 54 (1989) 1510

[46] T.P Nguyen, S.J. Lefrant, Phys. Cond. Matter 1 (1989) 5197

[47] K.C Smith, K.M. Black, Vac. Sci. Tec. A2 (1984) 744

[48] Z. Alizadeh, K. B. Sundaram, S. Seal. Appl Suface. Sci. 183 (2001) 270-277

[49] H. Li, S. Dimitrijev, D. Sweatman, H.B. Harrison, P. Tanner, B. Feil, J. of App. Phy. 86 (1999) 4316

[50] A. Tabata, Y. Kuno Y. Suzuoki, T. Mizutani, J. Phys. D 25 (1996) 194

[51] Z. Gong, E. G. Wang, G. C. Xu, Y. Chen, Thin Solid Films 348 (1999) 114

[52] R. C. Lee, C. R. Aita, N. C. Tran, J. Vac. Sci. Technol. A 9 (1991) 1351

[53] R.M Todi, K. B. Sundaram, Z. Alizadeh, A. P. Warren, K. Scammon, Solid State Elect., (to be published)

[54] Hartley M.A., Chiang J.N., Hess D.W., Soane D.S. Appl. Phys. Lett. 54, 1510 (1989)

[55] Nguyen T.P., Lefrant S. J. Phys. Cond. Matter 1, 5197 (1989)